UNIVERSITA' DEGLI STUDI DI TORINO

Doctoral School in Life and Health Sciences

PhD in Medical Pathophysiology

XXXVI CYCLE

PhD Thesis – Academic Year 2022-2023

Extracellular vesicles derived from Human Liver Stem Cells counteract chronic kidney disease development and cardiac dysfunction in remnant kidney murine model: the possible involvement of proteases

Tutor:

Prof.ssa Stefania Bruno

PhD candidate:

Dott.ssa Elena Ceccotti

Abstract

Chronic kidney disease (CKD) is a serious clinical hurdle without adequate therapeutic strategies to prevent its progression. The murine model of 5/6th partial nephrectomy with pole ligation (PNx) is the most suitable approach to mimic the human progressive renal failure and related uremic cardiomyopathy. In our group, we have demonstrated the therapeutic potential of extracellular vesicles (EVs) isolated from Human Liver Stem Cells (HLSCs) to counteract the progression of tissue fibrosis in different animal models of renal damage.

In this study, we performed the PNx two-step surgical procedure in 10-weeks-old SCID mice and the EVs were weekly administered starting 4 weeks after the nephrectomy, when signs of renal and cardiac chronic injuries were already evident. PNx mice were sacrificed 8 weeks after the second surgery.

We found that multiple HLSC-EV administrations exerted beneficial effects on renal function and morphology, by reducing interstitial fibrosis, glomerular sclerosis and capillary rarefaction. Moreover, we observed the statistically significant modulation of pro-fibrotic and pro-inflammatory markers in the renal tissue. Furthermore, the EV treatment ameliorated cardiac function and significantly reduced interstitial fibrosis, which is a key hallmark of diastolic dysfunction.

We also investigated the involvement of the proteases transported by EVs in their *in vivo* anti-fibrotic effect. Interestingly, EV-shuttled Matrix Metalloproteinase 1 (MMP1) seemed to be involved in their anti-fibrotic activity on renal tissue in PNx mice.

In conclusion, these data indicate that PNx mice developed both CKD and cardiac dysfunction. Multiple injections of different doses of HLSC-EVs can effectively improve renal and cardiac function and morphology, mainly through the reduction of tissue fibrosis. Moreover, at least in renal tissue, we demonstrated that HLSC-EV-shuttled proteases could be involved in their *in vivo* anti-fibrotic activity.

Table of contents

Introduction

Pathophysiology of Chronic Kidney Disease (CKD): the increased risk of developing cardiomyopathy

Chronic kidney disease (CKD) is a worldwide leading cause of mortality affecting more than 800 million of individuals (Kovesdy, 2022). Diabetes and hypertension are the main risk factors associated with CKD development and the symptoms worsen in association with other comorbidities. Glomerular filtration rate (GFR) is the best indicator of impaired kidney function, while tissue biopsy allows to highlight the histological hallmarks of CKD as glomerular sclerosis, interstitial fibrosis, capillary rarefaction and tubular atrophy (**Figure 1**). Other clinical complications associated with disease progression are proteinuria, anemia and systemic and glomerular hypertension. CKD may progress independently from the pathogenic triggers as result of a maladaptive processes of injury repair and of hemodynamic alterations due to nephron loss (Niculae *et al.*, 2023). When kidney function is severely compromised, end-stage renal disease (ESRD) may develop, increasing the risk of a premature death which is mainly caused by cardiovascular abnormalities, such as cardiac fibrosis and diastolic dysfunction (**Figure 1**) (Webster *et al.*, 2017).

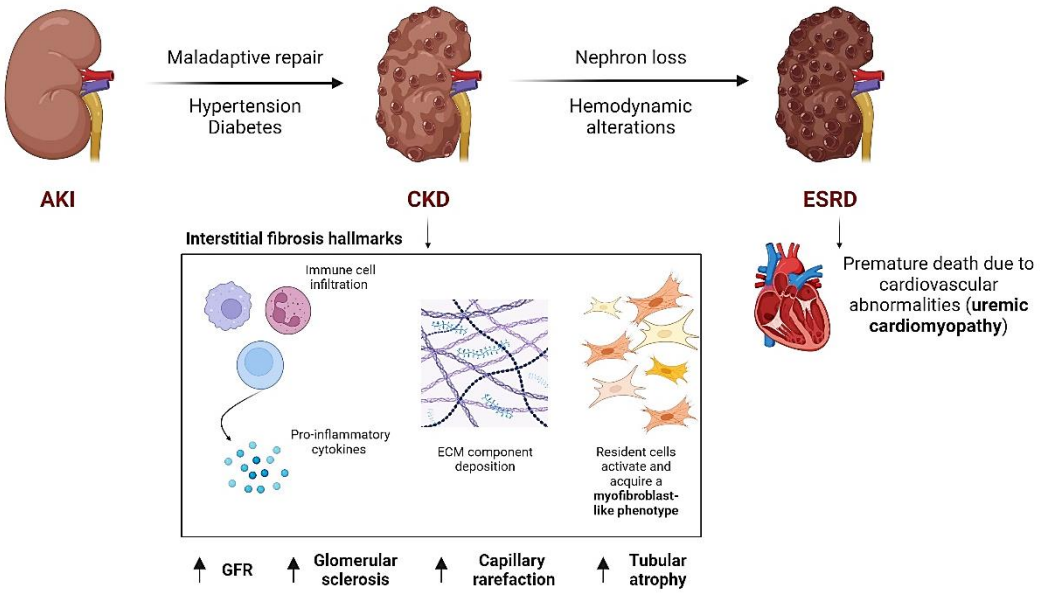

Figure 1. Pathophysiological features of CKD and transition to ESRD. The upper part of the figure shows the main causes which predispose to CKD and then to ESRD. The lower part of the figure illustrates the main pathophysiological alterations related to CKD development. Created with Biorender.com. Abbreviations: **AKI** (Acute Kidney Injury), **CKD** (Chronic Kidney Disease), **ESRD** (End Stage Renal Disease), **GFR** (Glomerular Filtration Rate).

In particular, uremic cardiomyopathy is diagnosed in many patients suffering from CKD which die within three years from the diagnosis and without any evident cardiac symptoms (Chen *et al.*, 2021) (Wang *et al.*, 2017). It is a clinical condition characterized by cardiovascular abnormalities, such as left ventricular hypertrophy (LVH), cardiac fibrosis and diastolic dysfunction (Chen *et al.*, 2021).

Renal fibrosis is considered a hallmark of CKD; it is, in fact, an independent contributor of disease progression (Leaf and Duffield, 2017). Fibrosis results from the infiltration of inflammatory cells and the activation of both resident cells of the interstitium (fibroblasts, pericytes and mesenchymal stem cells) and of the glomerulus (podocytes, parietal epithelial cells and mesangial cells) (Leaf and Duffield, 2017). These cells acquire a myofibroblast-like phenotype, thus they regulate the innate immune response and create a pro-fibrogenic niche by secreting pro-inflammatory mediators, as Transforming Growth Factor-beta (TGF-b) and cytokines (**Figure 1**) (Kholia *et al.*, 2018). Moreover, these events result in an imbalance in the deposition and degradation of extracellular matrix (ECM) components which accumulate around the arterioles, in the interstitial space and in the glomerular capillary walls, compromising the vasculature of the nephron (Leaf and Duffield, 2017) (Kholia *et al.*, 2018). In addition, the increased deposition of ECM components, such as Alpha-Smooth Muscle Actin (Alpha-SMA) and Collagen, subverts the kidney architecture (**Figure 1**) (Niculae *et al.*, 2023).

Stem cell-derived Extracellular Vesicles (EVs) as new therapeutic strategy to treat CKD

The actual standard of care for ESRD is only supportive and aims to slow the disease progression by replacing kidney function. Hospitalized patients mainly undergo hemodialysis and renal transplantation, but the benefits are respectively limited by the high costs and the poor donor availability (Abecassis *et al.*, 2008) (Grange, Skovronova *et al.*, 2019).

The worldwide incidence of CKD and its impact on the healthcare are increasing, for these reasons it is becoming extremely important to develop new therapeutic strategies (Kovesdy, 2022).

Mesenchymal stem/stromal cells (MSCs) are multipotent non-hematopoietic stem cells able to differentiate in multiple cell lineages. They show anti-fibrotic and immunomodulatory properties able to regenerate the damaged tissue in different animal models of organ injury (Picinich *et al.*, 2007) (Trohatou and Roubelakis, 2017) (Lu *et al.*, 2022) .The therapeutic potential of MSCs is related to the paracrine activity of MSC-released soluble factors, which includes Extracellular Vesicles (EVs) (Merimi *et al.*, 2021).

EVs are small membrane-nanoparticles involved in cell-cell communication both in physiological and pathophysiological conditions (Herrmann *et al.*, 2021).

Their bioactive cargo includes proteins, cytokines, growth factors, mRNA and non-coding RNAs. It reflects the cell of origin and is released in the target cell where it reprograms the molecular pathways involved in disease pathogenesis (**Figure 2**) (Birtwistle *et al.*, 2021).

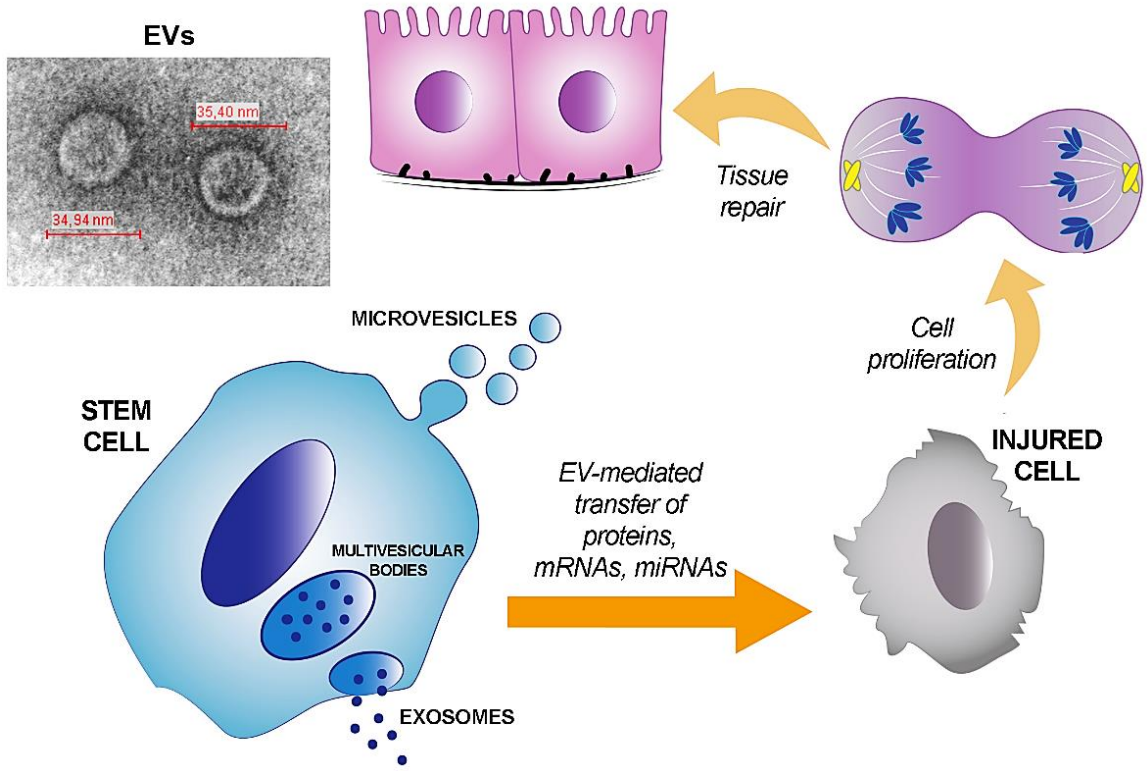

Figure 2. **Stem cell-derived EVs contribute to tissue repair.** Stem cell-derived EVs accumulate at the site of tissue injury and deliver proteins and specific patterns of mRNAs and miRNAs to injured cells. When incorporated into damaged cells, EVs activate regenerative programs, which accelerate tissue recovery. Inset: representative transmission electron microscopy image of EVs (original magnification 250.000).
Figure from *Bruno S., et al. Role of extracellular vesicles in stem cell biology. Am J Physiol Cell Physiol. 2019.* Abbreviations: **mRNA** (messenger RNA), **miRNA** (microRNA).

EVs derived from different types of stem cells, in particular those derived from MSCs, are able to mimic the beneficial effects of the cells of origin in experimental *in vivo* models of tissue injury (Bruno *et al.*, 2009) (Herrera *et al.*, 2014) (Monsel *et al.*, 2015).

Human liver stem cells (HLSCs) are multipotent MSC-like cells isolated from healthy human adult liver donors under stringent culture conditions (**Figure 3A**) (Herrera *et al.*, 2006).

As shown in **Figure 3B and 3C,** HLSCs co-express some mesenchymal markers (CD29, CD73, CD44, and CD90) and liver-specific markers (cytokeratin-8 and -18, albumin and α-fetoprotein) which suggest the mesenchymal origin of these cells and their hepatic lineage commitment (Herrera *et al.*, 2006). Moreover, HLSCs express the common stem cell (vimentin and nestin) and embryonic stem cell markers (Oct3/4, Nanog, SSEA4, Sox2, and Musashi1), which are related to their self-renewal capacity and multipotency (**Figure 3B and 3C)** (Herrera *et al.*, 2006). Interestingly, HLSCs are negative for the hematopoietic markers (CD34, CD45, CD117, and CD133), the human leukocyte antigen class II (HLA-II) and the costimulatory molecules (CD40, CD80, and CD86) (**Figure 3C)** (Herrera *et al.*, 2006) (Bruno *et al.*, 2016).

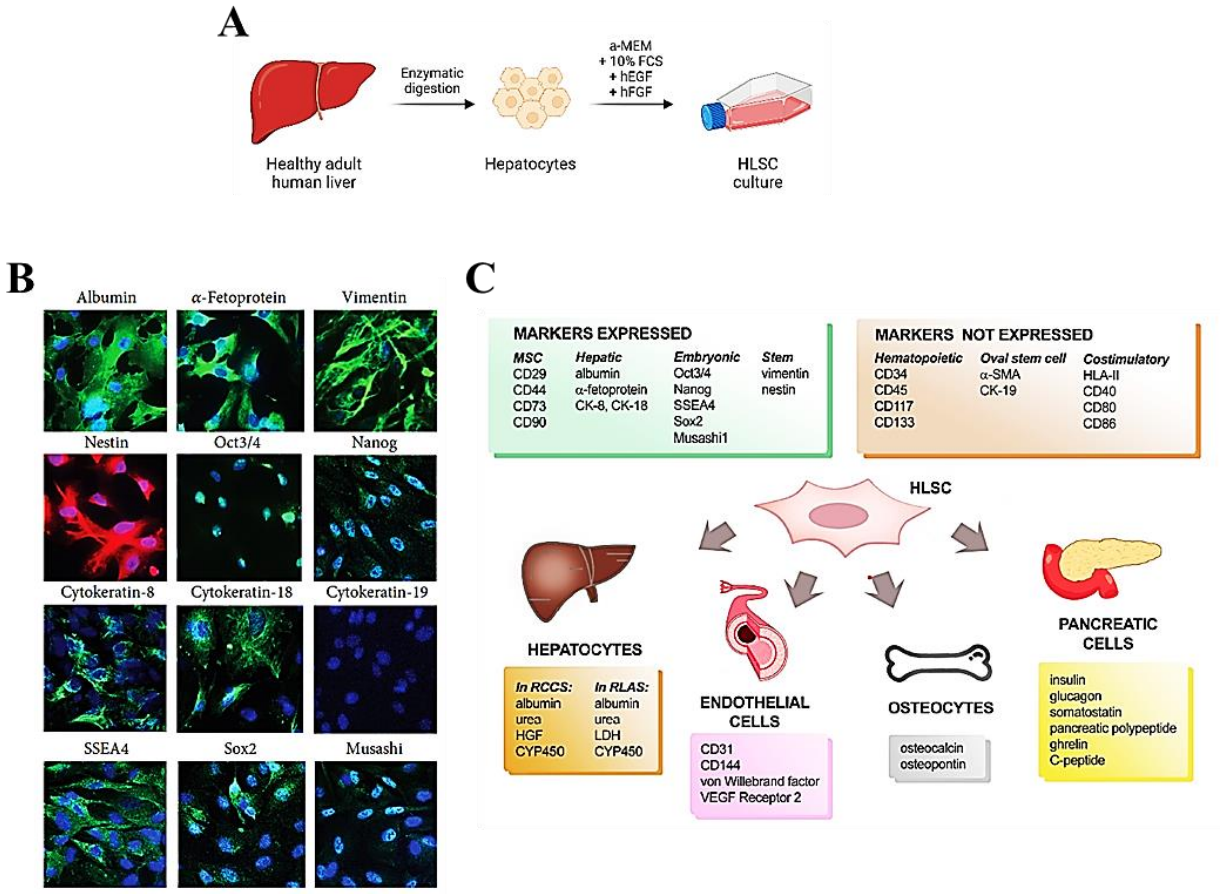

Figure 3. HLSC isolation and characterization. **A**) Schematic representation of HLSC isolation protocol. Created with Biorender.com. **B**) Confocal micrographs showing the expression of hepatic, mesenchymal, and embryonic stem cell markers in HLSCs (original magnification at × 400). Figure from *Bruno S. et al. Human Liver-Derived Stem Cells Improve Fibrosis and Inflammation Associated with Nonalcoholic Steatohepatitis. Hindawi, 2019.* **C**) HLSC phenotypic characterization and differentiation. Figure from *Bruno S. et al. Human Liver Stem Cells: A Liver-Derived Mesenchymal Stromal Cell-Like Population with Pro-Regenerative Properties. Front. Cell Dev. Biol. 2021.* Abbreviations: **HLSC** (Human Liver Stem Cell).

HLSCs constitutively expressed cyclooxygenase 1 and indoleamine 2,3-dioxygenase; in fact, they show immunomodulatory properties by inhibiting T-cell proliferation, dendritic cells (DCs) differentiation and Natural Killer cell (NK) activity (Bruno *et al.*, 2016).

The therapeutic properties of HLSCs were evaluated in a murine model of acute liver injury (ALI), where they participated in the regeneration of liver parenchyma (Herrera *et al.*, 2006), and in a mouse model of non-alcoholic steatohepatitis (NASH), where HLSCs improved liver function and morphology, but also reduced tissue inflammation and fibrosis (Bruno *et al.*, 2019).

Apart from liver damage, HLSCs improved renal tissue regeneration in different mouse models of acute kidney injury (AKI); in particular, in a glycerol-induced AKI model, they reduced tubular necrosis and induced tubular cell proliferation (Herrera *et al.*, 2014).

HLSC-derived extracellular vesicles (HLSC-EVs) act as paracrine effectors and they are able to mediate the therapeutic properties of the cell of origin by transferring active biological materials protecting the damaged tissue (Bruno *et al.*, 2021).

In our group, we have focused our attention on understanding the *in vivo* capacity of HLSC-EVs to modulate tissue regeneration, inflammation and fibrosis. In the last years, we have studied the possible therapeutic implications of EV-based treatments as a cell-free strategy to treat tissue fibrosis in different animal models of liver and kidney damage.

HLSC-EVs, for example, improved liver function and reduced liver fibrosis and inflammation at both morphological and molecular levels by downregulating the expression of pro-fibrotic genes (Bruno *et al.*, 2020).

On the other hand, in a murine model of diabetic nephropathy (DN), the injection of HLSC-EVs reduced both interstitial fibrosis and glomerular sclerosis (Grange, Tritta *et al.*, 2019) and prevented the progression of aristolochic acid (AA)-induced kidney fibrosis (Kholia *et al.*, 2018). Moreover, in a model of ischemia and reperfusion injury (IRI), treatment with HLSC-EVs was able to interfere with the development of acute-on-chronic kidney disease by modulating genes involved in epithelial-to-mesenchymal transition (EMT) (Bruno *et al.*, 2022).

CKD animal models: a special focus on 5/6 partial nephrectomy (PNx) murine model

In the last years, different CKD animal models have emerged in the attempt of recapitulating the main pathological alterations occurring in humans. Among them, the 5/6 nephrectomy model is widely diffused due to its ability to mimic the progressive renal failure after the loss of kidney mass in human

patients (Tan *et al.*, 2019). The conventional subtotal nephrectomy, the so-called ablation model, includes the removal of one kidney and the excision of the 2/3rd of the other kidney. This surgical procedure is associated with excessive post-operative bleeding and animal mortality (Tan *et al.*, 2019). Recently, a new surgical procedure has been introduced: the 5/6th partial nephrectomy model with pole ligation (PNx). It consists of a two-step surgery; at first, the upper and lower poles of the left kidney are ligated and one week after, the right kidney is removed (**Figure 4**) (Wang *et al.*, 2017).

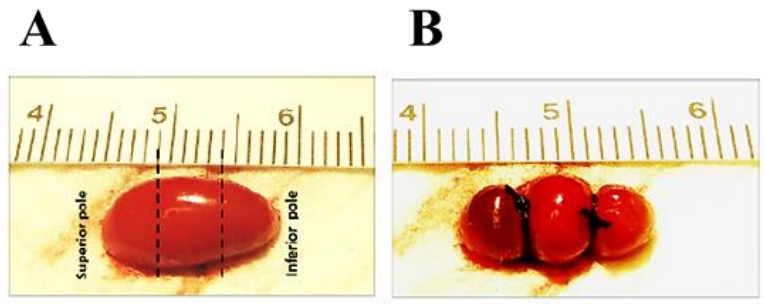

Figure 4. 5/6th partial nephrectomy (PNx) experimental procedure. Left kidney before (**A**) and after (**B**) pole ligation. Figure from *Wang X. et al. A Mouse 5/6th Nephrectomy Model That Induces Experimental Uremic Cardiomyopathy. Jove. 2017.*

The PNx procedure has been initially developed in rats because they are easier to handle, but murine models have been recently introduced, considering the easier way to genetically manipulate them (Chen *et al.*, 2021). The surgical micromanipulations are not always feasible in mice, but it significantly reduces the mortality rate with respect to the conventional subtotal nephrectomy model (Tan *et al.*, 2019).

The PNx animals are sacrificed both 4 and 12 weeks after the second surgery; at this time, the upper and lower poles of the left kidney become necrotic and have been almost absorbed, leaving 1/3rd of a single kidney (Wang *et al.*, 2017). One month after the second surgical intervention, the animals spontaneously develop the common hallmarks of CKD, as tubulointerstitial fibrosis, glomerular sclerosis and uremic cardiomyopathy (Wang *et al.*, 2017).

The involvement of EV-associated proteases in disease progression

Matrix metalloproteinases (MMPs) are an enzyme family that, under normal physiological conditions, maintain tissue allostasis by catalyzing the turnover of the ECM components.Thus, they can contribute to embryogenesis, tissue remodeling and wound healing, but an imbalanced MMP expression or activity can have important consequences in several diseases, such as cancer, cardiovascular disease, inflammatory disease, nephritis, tissue ulcers and, fibrosis (Serra, 2020) (Visse and Nagase, 2003). Recent studies highlighted the presence of different EV-associated MMPs, such as surface-bound and soluble MMPs, a disintegrin and a metalloproteinase (ADAMs) and tissue inhibitor of metalloproteinases (TIMPs) (Shimoda and Khokha, 2017). It has been reported that EV-associated MMPs can directly contribute to ECM degradation in tumors, where they contribute to the EV ability of remodeling the ECM components and thus favoring tumor invasion (**Figure 5**) (Shimoda and Khokha, 2017) (Zucker *et al.*, 1987).

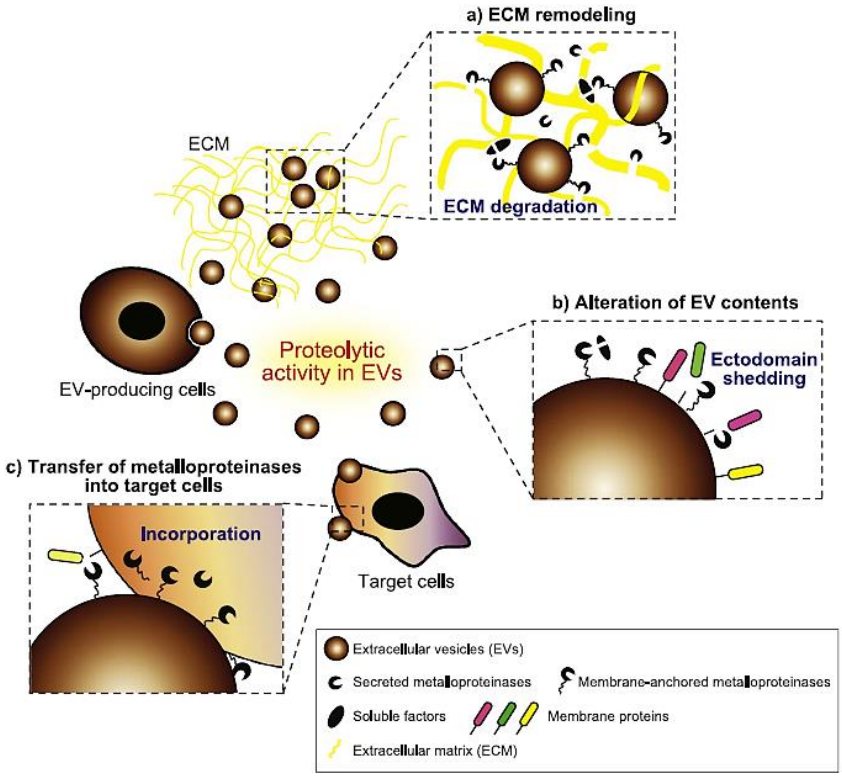

Figure 5. Possible functions of EV-associated metalloproteinases. Experimental evidences suggest the possible functions of EV-associated metalloproteinases: **a**) tissue microenvironment remodeling by ECM degradation, **b**) alteration of the EV contents by ectodomain shedding, and **c**) transfer of EV-associated metalloproteinases into target cells. Figure from *Shimoda M. et al. Metalloproteinases in extracellular vesicles. BBA - Molecular Cell Research. 2017.* Abbreviations: **ECM** (Extracellular Matrix).

Aim of the work

We set up a murine model of 5/6th PNx to investigate the development of CKD and related uremic cardiomyopathy, as occurs in human patients. The injection of different doses of HLSC-EVs was weekly performed in PNx mice, starting at week 4 after the nephrectomy, when signs of renal and cardiac chronic injuries were already evident.

We tested the therapeutic effects of HLSC-EVs both on the remnant kidney and on the heart, at histological, functional and molecular level.

We investigated the contribution of ECM remodelling-related proteases to the anti-fibrotic effect of HLSC-EVs.

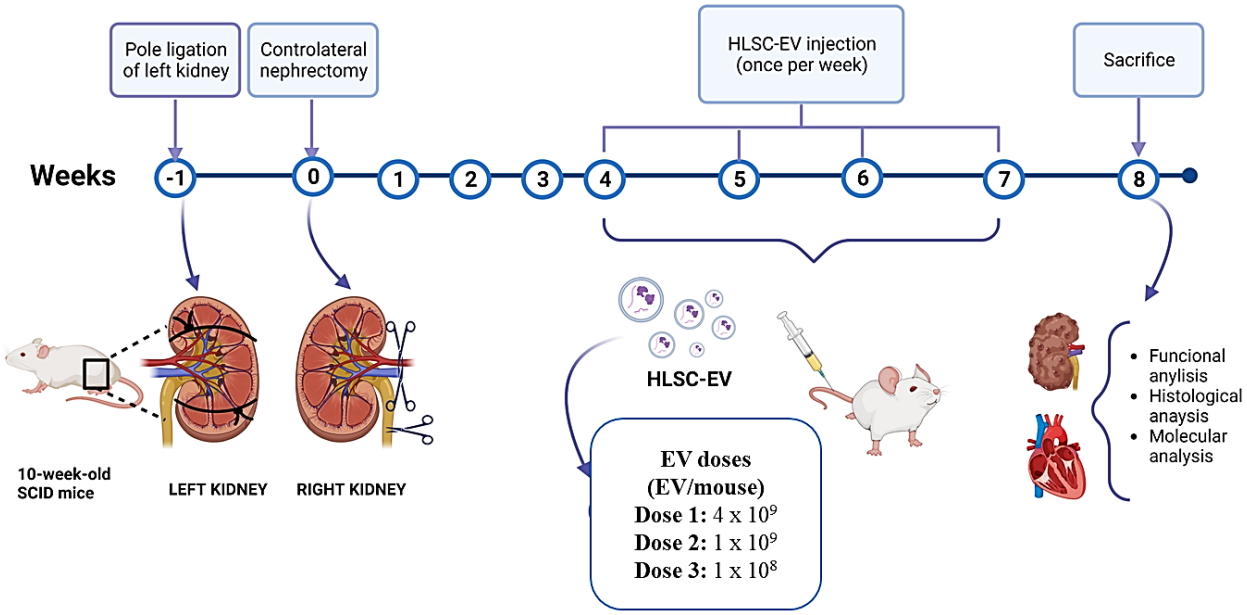

Figure 6. Schematic representation of the experimental procedure. Created with Biorender.com.

Material and Methods

Isolation and characterization of HLSC-EVs

HLSCs were isolated and characterized as previously reported (Herrera *et al.*, 2006) (Bruno *et al.*, 2019) (Spada *et al.*, 2020). HLSCs were maintained in Minimal Essential Medium (α-MEM) with 10% Fetal Calf Serum (both purchased from Euroclone, Pero, MI, IT), 10ng/mL of human recombinant Epidermal Growth Factor, 10ng/mL of human recombinant Fibroblast Growth Factor basic (Miltenyi, Bergisch Gladbach, Germany), 2nM L-Glutamine (Lonza, Basel, CH), and antibiotics (100U/mL of Penicillin/Streptomycin, Sigma-Aldrich, St. Louis, MO, USA). HLSCs were used until passage 8 and plated at a density of $2.5x10^5$ cells per flask (T75, Corning, VWR International, Milano, Italy).

EVs were isolated from the supernatants of sub-confluent HLSCs cultured in hyperflasks (Corning) at a density of 3000 cells/cm^2 for 18h in serum-free conditions. The next day, cell supernatant was collected, centrifuged at 3000g for 15min to eliminate cell debris and dead cells, and passed through 0.22μm filters to exclude apoptotic bodies and large vesicles. EVs were purified by ultracentrifugation at 100,000g for 2h at 4°C (Beckman Coulter Optima L-100 K, Fullerton, CA, USA). The pellet was resuspended in RPMI supplemented with 1% dimethyl sulfoxide (DMSO, Sigma-Aldrich) and stored at -80°C for subsequent studies.

Each EV preparation was diluted in saline solution (1:100) and quantified using the NanoSight NS300 instrument (NanoSight Ltd., Amesbury, United Kingdom), equipped with a 405nm laser. For each EV preparation, the recordings of three 60-s videos were analyzed under constant flow conditions (flow rate = 30) using nanoparticle tracking analysis (NTA) software v.3.2, as previously described (Bruno *et al.*, 2020).

HLSC-EV phenotype was characterized by cytofluorimetric analysis using a bead-based multiplex analysis system (MACSPlex Exosome Kit, human, Miltenyi Biotec, Bergisch Gladbach, Germany), as reported in previous studies (Koliha *et al.*, 2016) (Wiklander *et al.*, 2018) (Bruno *et al.*, 2020).

Briefly, $2x10^9$ EVs were diluted with MACSPlex buffer and incubated with MACSPlex Exosome Capture Beads for 18h at 450rpm, to allow EV binding to 39 different antibody-coated bead subsets. Counterstaining was carried out by incubating the EVs that were bound by capture beads with the APC-conjugated anti-CD63, anti-CD81, and anti-CD9 detection antibodies for 1h at 450rpm, protected from light. Washing steps with MACSPlex buffer were performed to remove the unbound antibodies. Approximately 5000 single beads per sample were acquired using a Cytoflex flow cytometer (Beckman Coulter, Brea, CA, USA). The CytExpert Software was employed to identify and gate all bead populations based on their respective fluorescence intensity. The median fluorescence intensity (MFI) was calculated for each capture bead subset and the background fluorescence intensity was removed by subtracting the MFI value of a blank control that was processed in the same way as the EV samples (medium + capture beads + detection antibodies) from the MFI of all the 39 capture bead subsets.

To evaluate EV size and integrity, transmission electron microscopy (TEM) was performed on $3x10^9$ EVs fixed on 200 mesh nickel formvar carbon-coated grids (Electron Microscopy Science, Hatfield, PA, United States) and then, left to adhere for 20min, as earlier reported (Deregibus *et al.*, 2016).After washing with PBS, the grids were incubated with 2.5% glutaraldehyde containing 2% sucrose and they were extensively washed in distilled water. Finally, the EVs were negatively stained using Nano-W™ and NanoVan™ (Nanoprobes, Yaphank, NY, USA) and observed using a JEM-1400 Flash transmission electron microscope (JEOL, Tokyo, Japan).

Protease array

For protease analysis inside EVs, an iodixanol floating separation protocol was applied to further purify EV preparations from contaminating proteins and RNAs, as previously described (Kowal *et al.*, 2016) (Ranghino *et al.*, 2017) (Chiabotto *et al.*, 2021). Briefly, EV pellets were resuspended with a mixture of 60% iodixanol (Optiprep from Sigma-Aldrich) and 0.25M sucrose. Over this EV-containing

preparation, iodixanol gradients at 30, 15 and 5% were layered in each polycarbonate centrifuge tube (Beckman Instruments). The tubes were ultracentrifuged at 350.000g at 4°C for 1h without breaking. The 15 and 30% fractions were recovered, pooled, and diluted in phosphate-buffered saline (PBS), and ultracentrifuged again at 100,000g for 1h. The pellet was resuspended in RPMI with 1% DMSO and stored at –80°C.

To characterize the expression profile of 35 human proteases in HLSCs and HLSC-EVs, the Proteome Profiler™ Human Protease Array Kit (R&D Systems, Minneapolis, Minnesota, USA) was used following the manufacturer's instructions. In this assay, capture and control antibodies have been spotted in duplicate on nitrocellulose membranes. HLSC and EV lysates (200µg) were mixed with a cocktail of biotinylated detection antibodies and incubated overnight with the Proteome Profiler™ Human Protease Array membranes. After removing the unbound materials, streptavidin-HRP and chemiluminescent detection reagent were applied. Pixel density was determined using Chemidoc and Image Lab analysis software (Bio-Rad, Hercules, CA, USA). After calculating the average signal of the pairs of duplicate spots, the background signal was subtracted from each spot average. As background, the negative control spot average was considered.

Western blot analysis

HLSCs and HLSC-EVs were lysed at 4°C for 3min in Lysis Buffer 17 supplemented with 10µg/ml Aprotinin, 10µg/ml Leupeptin and 10µg/ml Pepstatin (all purchased from R&D Systems, Minneapolis, Minnesota, USA).

Protein concentration was assessed using the bicinchoninic acid (BCA) Protein Assay Kit (Pierce™ Thermo Fisher, Waltham, MA, USA) and 5µg of the protein samples were analyzed as previously described (Chiabotto *et al.*, 2021). Briefly, 4–20% gradient mini-PROTEAN TGX precast electrophoresis gels (Bio-Rad, Hercules, CA, USA) were used to separate proteins under reducing conditions, before transferring them onto 0.2µm nitrocellulose membranes. After saturation in Clear

Milk Blocking Buffer (Pierce™ Thermo Fisher) for 2h at room temperature , membranes were probed at 4°C over-night with specific rabbit anti-human primary antibodies: anti-ADAM9, anti-MMP1, anti-MMP2, anti-CD26, anti-urokinase-type plasminogen activator (uPA), anti-CD63, anti-CD81, anti-CD9 and anti-GM130 (all purchased from Cell Signaling Technology (Danvers, MA, United States)) and all used with a dilution of 1:1000 in phosphate-buffered saline (PBS) supplemented with 0.1% Tween-20 (PBS-T) and 5% bovine serum albumin. Then, membranes were incubated for 1h at room temperature with an anti-rabbit HRP-conjugated secondary antibody (Thermo Fisher Scientific), with a dilution of 1:5000 in PBS-T. After incubation with the enhanced chemiluminescence substrate (SuperSignal™ West Femto Maximum Sensitivity Substrate, Thermo Fisher Scientific), the chemiluminescent signal was detected using the Chemidoc system (Bio-Rad) and band intensity was evaluated using Image Lab software (Bio-Rad).

Partial nephrectomy 5/6th murine model

Animal studies were conducted in accordance with the National Institute of Health Guide for the Care and Use of Laboratory Animals. The procedures were approved by the Italian Health Ministry (authorization number: 275/2021-PR). Ten-week-old male SCID mice were purchased from ENVIGO (S. Pietro al Natisone, Udine Italy).

The partial nephrectomy 5/6th (PNx) procedure was performed by a two-step surgery as previously described (Wang *et al.*, 2017) (Tan *et al.*, 2019). In step one, the animal was anesthetized by intramuscular administration of Zolazepam (80mg/kg, Virbac, Milano, Italy) and Xylazine (16mg/kg, Bayer, Milano, Italy) under sterile conditions. The left lumbar area was prepared for surgery by performing a trichotomy followed by disinfection with Iodopovidone (Esoform Manufacturing, Rovigo, Italy). The animal was then placed on the right side on a heating plate to maintain the body temperature at 37°C. A lumbar incision was performed, and the superior and inferior poles of the left kidney were then ligated using a 4-0 silk suture (Fine Science Tools GmbH, Heidelberg Germany). In

step two, performed 1 week after step one, the right kidney was treated in the same way as the left kidney through the procedure mentioned above. In addition, using angled forceps, a double ligation of the right kidney ureter was carried out before dissecting it. This prevents urine from entering the peritoneum from the bladder through the right dissected ureter. To ligate the blood vessels with 6/0 silk suture (Ethicon Raritan, New Jersey USA), an access channel was created under the artery and the renal vein using angular forceps. Following the correct occlusion of the blood vessels, nephrectomy was performed. After surgery, the muscle and skin were closed with 6-0 silk sutures (Ethicon), and the surgical area was disinfected with Iodopovidone (Esoform). Afterwards, the mouse was housed in a designated cage under a heat lamp at 37°C for 20min.

A control group of mice (SHAM) was subjected to all procedure describe above without ligation of the poles (superior and inferior) of the left kidney and without nephrectomy of the right kidney.

To set up the experimental protocol, PNx mice were sacrificed 4 and 8 weeks (n=8/experimental point) after the second surgery (**Figure 7A**). To evaluate the effect of EV treatment, 4 weeks after the contralateral nephrectomy, the PNx mice that survived the surgical procedures were randomly divided and treated with vehicle alone (n=10) or with different amounts of EVs, once a week for four weeks. Different doses of EVs have been administered: $4x10^9$ EV/mice/administration (dose 1, n=10), $1x10^9$ EV/mice/administration (dose 2, n=6) and $1x10^8$ EV/mice/administration (dose 3, n=6). A group pf PNx mice (n=6) received the dose 1 pretreated with neutralizing anti-human MMP1 antibody (200µg/ml, R&D Systems). Mice were sacrificed two months after the nephrectomy and blood, remnant kidney and heart have been recovered for analyses.

Renal functional and histological analysis

The renal function has been assessed by biochemical analyses. Creatinine plasma levels were determined using a colorimetric microplate assay that was based on the Jaffe reaction (QuantiChrom™ Creatinine Assay Kit, BioAssay Systems, Hayward, CA, United States). The levels of blood urea

nitrogen (BUN) were evaluated by measuring serum urea with a colorimetric assay kit, following manufacturer's protocol (Arbor Assays, Ann Arbor, MI, United States).

The kidney morphology was assessed using formalin-fixed paraffin-embedded tissue staining. Five micrometer paraffin sections were routinely stained with Masson's trichrome (Bio-Optica, Milan, IT) or Periodic Acid Schiff (PAS, Bio-Optica) staining according to the manufacturer's instructions.

The surface area that was occupied by collagen fibers was quantified in 10 random non-overlapping HPFs per section from images that were taken at a magnification of 400x, and multiphase image analyses were carried out using ImageJ software version 1.49s.

The glomerular deposition of the PAS positive extracellular matrix was determined by ImageJ software on 15 glomeruli from each mouse at a magnification of 400X.

Renal sections from paraffin-embedded blocks were stained using goat anti-mouse CD31 antibody (Biotechne, Minneapolis, MN, United States). Endogenous peroxidase activity was blocked with 6% hydrogen peroxide for 8min at room temperature. After antigen retrieval by boiling in ethylenediamine tetraacetic acid (EDTA) buffer (pH 9), primary antibody (1:100) was applied to slides over-night at 4°C. Horseradish peroxidase-labeled anti-goat antibody (Thermo Fisher Scientific) were incubated for 1h at room temperature. The reaction product was developed using 3,3-diaminobenzidine. Omission of the primary antibody served as negative control.

Transmission electron microscopy (TEM) of renal tissue

Kidneys were freshly dissected out from SHAM mice (n = 3), PNx mice sacrificed 8 weeks after the nephrectomy treated with vehicle alone (n = 3) or with EV dose 1 (n = 3). Renal tissue was cut in small pieces (1-2 mm thick) and fixed by immersion in 2.5 % glutaraldehyde in phosphate buffer (PB, 0.1M, pH7.4) for 48h at 4°C.

After washing in PBS, they were post-fixed in osmium ferrocyanide (1 volume of 2% aqueous osmium tetroxide: 1 volume of 3% potassium ferrocyanide) for 1h at 4 °C. Then, the samples were dehydrated

for 15min in increasing concentrations of acetone (30%, 60%, 90%, 100%), incubated in acetone 100%/Spurr resin (1:1, 30min, 1:2, 30min) and in Spurr resin (Electron Microscopy Sciences) overnight at room temperature. Finally, they were embedded in Spurr resin using 0.5ml Eppendorf tubes for 24h at 70°C.

Ultrathin sections were cut with an ultramicrotome (EM UC6, Leica Microsystems, Milan, Italy), collected on uncoated nickel grids (100 mesh) and counterstained for 30s with UranyLess EM Stain and 30s with lead citrate (Electron Microscopy Sciences). Sections were observed with a JEM-1400 Flash transmission electron microscope (JEOL, Tokyo, Japan) and images acquired with a high sensitivity sCMOS camera (JEOL).

Molecular analysis of renal tissue

The total RNA was extracted from the renal tissue of the SHAM or PNx-mice that were treated or not with HLSC-EVs using TRIzol™ reagent (Ambion, Thermofisher, Waltham, MA, United States), following the manufacturer's instructions. TRIzol™ solutions were homogenized using Bullet Blender (Next Advance Inc., New York, NY, United States) and 0.5mm zirconium oxide beads at a speed of 8rpm for 3min. After centrifugation at 12,000g for 10min at 4°C, the RNA was purified from the supernatant and then quantified spectrophotometrically (mySPEC, VWR, Radnor, PA, United States). A High-Capacity cDNA Reverse Transcription Kit (Applied Biosystems, Foster City, CA, United States) was used to convert RNA into complementary DNA (cDNA). To evaluate specific gene expression by quantitative Real-Time PCR (qRT-PCR), a 96-well QuantStudio^{TM} 12K Flex Real-Time PCR system (Thermo Fisher Scientific) was used. In each well we loaded 20µL reaction mixture containing Power SYBR Green PCR Master Mix (Applied Biosystems), 10ng of sample cDNA, and sequence-specific oligonucleotide primers (100nM, purchased from MWGBiotech, Eurofins Scientific, Brussels, Belgium). See **Table 1** for the primers used for qRT-PCR.

To normalize qRT-PCR data, GAPDH was used as housekeeping gene. For all samples, fold-change expression with respect to the PNx group or the SHAM group was calculated using ΔΔCt method.

Table1. Primer pairs used for the detection of murine genes by qRT-PCR.

Gene name	Forward (5'-3')	Reverse (5'-3')
GAPDH	TGTCAAGCTCATTTCCTGGTA	TCTTACTCCTTGGAGGCCATGT
Alpha-SMA	CATCTCCGAAGTCCAGCACA	GACGCACCACTGAACCCTAA
COL1A1	ACCTTGTTTGCCAGGTTCAC	ATCTCCCTGGTGCTGATGGAC
IL-6	ACCAGAGGAAATTTTCAATAGGC	TGATGCACTTGCAGAAAACA
TGF-beta	GCAACAATTCCTGGCGTTACC	CGAAAGCCCTGTATTCCGTCT
TNF-alpha	CATCTTCTCAAAATTCGAGTGACAA	TGGGAGTAGACAAGGTACAACCC

Cardiac histological analyses

Hearts were sectioned transversely to include the right and left ventricles, emphasizing their morphology and the endocardium-to-epicardium transition. Structural damage to the heart was assessed through histopathological analysis. Two pathologists evaluated and reported histopathological (e.g., atrophy, inflammation, necrosis, fibrosis) characteristics.

Pathology features were recorded and graded based on the extent (none, mild, moderate, severe), distribution (focal, multifocal, or diffuse), and subsite location (epicardium, myocardium, endocardium) (Jokinen *et al.*, 2005) (Jokinen *et al.*, 2011) (Ishibashi-Ueda *et al.*, 2017). In particular, cardiomyocyte atrophy was defined as cell size decrease. In addition, as the heart is considered an immune "sanctuary", the presence of any inflammatory cells within the cardiomyocytes was considered pathological and was recorded. Cardiomyocytes with cytoplasmic eosinophilia and nuclear loss accompanied by interstitial edema or loss of myocardial fibers were considered for necrosis assessment and graded. Finally, cardiac fibrosis was reported and further differentiated in interstitial (fibrotic bundles outlining cardiomyocytes), replacement/scaring (fibrotic deposits replacing injured/necrotic cardiomyocytes), and perivascular (fibrotic tissue surrounding capillaries and small vessels) fibrosis (Gürtl *et al.*, 2009) (Gay-Jordi *et al.*, 2013).

Transthoracic Echocardiography

Mice were anesthetized with 1% isoflurane and analyzed with a Vevo 2100 High Resolution Imaging System (Visual Sonics Inc, Toronto, Canada) equipped with a 30MHz probe (MS550D) (VisualSonics, Toronto, Canada). Left ventricle mass, left ventricle internal diameters (LVID) and interventricular septum thickness (IVS) were measured at the level of the papillary muscles in the parasternal short-axis view (M mode). Mitral valve deceleration time was measured with tissue Doppler and pulsed wave Doppler techniques in the apical long-axis view. All measurements were averaged on 3 consecutive cardiac cycles per experiment and cardiac function was assessed when heart rate was 400-450bpm.

Statistical analyses

Statistical analysis was performed using GraphPad Prism software version 8.0 (GraphPad Software, Inc., CA, USA). All data were displayed as mean ± SD. Analysis of variance (ANOVA) was applied for data analysis and a p-value of <0.05 was considered significant.

Results

Set up of the *in vivo* model of CKD

As previously described (Wang *et al.*, 2017), in PNx animals sacrificed 4 weeks after the second surgery, the upper and lower poles of the left kidney became necrotic and have been almost absorbed, leaving 1/3rd of a single kidney. Biochemical analyses of markers of renal dysfunction pointed out an increase in creatinine (**Figure 7B**) and BUN (**Figure 7C**) plasma levels in mice subjected to PNx and sacrificed 4 weeks after the nephrectomy, with respect to SHAM mice. PNx mice sacrificed 8 weeks after the nephrectomy had a further significant increase in BUN and creatinine plasma levels, indicating a worsening of kidney function (**Figure 7B and 7C**).

At histological level, PNx-mice sacrificed 4 and 8 weeks after the nephrectomy showed signs of CKD development: in particular, the presence of interstitial fibrosis was observed at both timings (**Figure 7F**). Quantification of the fibrotic area indicated that a significant increase in fibrosis was already detectable in PNx mice 4 weeks after the second surgery, compared to SHAM mice (**Figure 7D**). At glomerular level, we observed an increase in glomerular size (**Figure 7G**) and in glomerular deposition of periodic acid-Schiff (PAS) positive extracellular matrix (**Figure 7E**), thus indicating glomerulosclerosis development.

Molecular analysis of genes known to be involved in the development of fibrosis demonstrated that PNx mice sacrificed at 4 and 8 weeks after the nephrectomy exhibited a significant increase in Alpha-Smooth Muscle Actin (alpha-SMA) and collagen I (COL1A1) gene expression levels (**Figure 7H and 7I**). Gene expression level of transforming growth factor beta 1 (TGF-beta) increased at week 8 but did not reach a statistically significant difference.

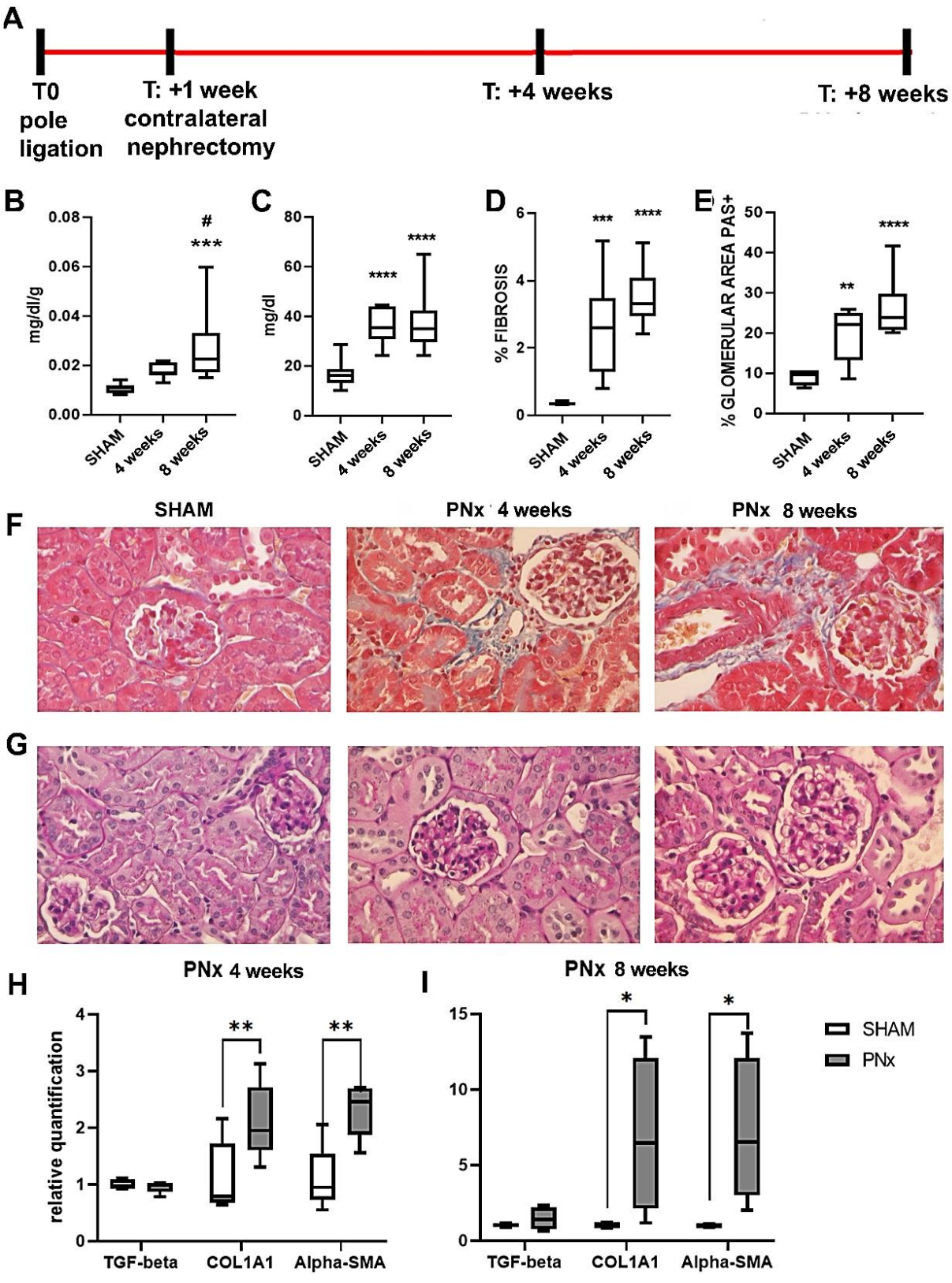

Figure 7. CKD development in 5/6th partial nephrectomy (PNx) model. A) Schematic representation of the experimental design to set up the *in vivo* model. At T0, mice were subjected to pole ligation of the left kidney. One week after (T +1) the right kidney was removed (contralateral nephrectomy). The mice were sacrificed 4 and 8 weeks after the second surgery to evaluate CKD development. **B and C)** Evaluation of creatinine (**B**) and BUN (**C**) plasma levels of control SHAM mice (n=12) and of PNx mice sacrificed 4 and 8 weeks after the nephrectomy (n=8/time point). Results are shown as mean ± SD. Ordinary One Way ANOVA with Tukey's multiple comparison test was performed by Prism. For creatinine

plasma level: ***p<0.001 PNx mice sacrificed 4 weeks after the nephrectomy *versus* SHAM mice; # p<0.05 PNx mice sacrificed 8 weeks after the nephrectomy *versus* PNx mice sacrificed at week 4. For BUN plasma level: ****p<0.0001 PNx mice sacrificed 4 or 8 weeks after the nephrectomy *versus* SHAM mice. **D)** Histological quantification of fibrosis in SHAM and in PNx mice sacrificed 4 and 8 weeks after the nephrectomy, by multiphase image analysis of 10 fields per section. Results are shown as mean ± SD. Ordinary One Way ANOVA with Tukey's multiple comparison test was performed by Prism. ****p ≤ 0.0001 PNx mice sacrificed 8 weeks after the nephrectomy *versus* SHAM mice; ***p ≤ 0.0007 PNx mice sacrificed 4 weeks after the nephrectomy *versus* SHAM mice. **E)** Histological quantification of glomerular PAS+ deposition in SHAM and in PNx mice sacrificed 4 and 8 weeks after the nephrectomy, by multiphase image analysis using ImageJ software on at least 15 glomeruli from each renal section stained with PAS (magnification: 400X). Results are shown as mean ± SD. Ordinary One Way ANOVA with Tukey's multiple comparison test was performed by Prism. ****p ≤ 0.0001 PNx mice sacrificed 8 weeks after the nephrectomy *versus* SHAM mice; **p ≤ 0.005 PNx mice sacrificed 4 weeks after the nephrectomy *versus* SHAM mice. **F)** Representative micrographs of Masson's trichrome stained renal sections of SHAM and PNx mice sacrificed 4 and 8 weeks after the nephrectomy. The blue stain represents collagen fibers considered a marker for renal interstitial fibrosis. Original magnification 400×. **G)** Representative micrographs of PAS-stained renal sections of SHAM and PNx mice sacrificed 4 and 8 weeks after the nephrectomy. Original magnification 400×. **H)** Gene expression levels of fibrotic markers (TGF-beta, COL1A1 and Alpha-SMA) in PNx mice sacrificed 4 weeks after the nephrectomy (n=5/group) and in SHAM mice (n=5). Data are normalized to GAPDH. Mean ± SD was calculated by comparing the gene expression levels of each group with the ones of the SHAM mice. Statistical analysis was performed using the Two-way ANOVA with Sidak multiple comparison test by Prism: **p ≤ 0.01 PNx mice *versus* SHAM mice for COL1A1 and alpha-SMA. **I)** Gene expression levels of fibrotic markers (TGF-beta, COL1A1, and Alpha-SMA) in PNx mice sacrificed 8 weeks after the nephrectomy (n=4) with respect to SHAM mice (n=4). Data are normalized to GAPDH. Mean ± SD was calculated by comparing the gene expression levels of each group with the ones of the SHAM mice. Statistical analysis was performed using the Two-way ANOVA with Sidak multiple comparison test by Prism: *p ≤ 0.03 PNx mice *versus* SHAM mice for COL1A1 and alpha-SMA.

HLSC-EV characterization

HLSC-EVs were isolated as reported in the section 'materials and methods'. As previously described (Andreu and Yáñez-Mó, 2014), HLSC-EVs expressed tetraspanins (CD63, CD81, and CD9) (**Figure 8A and 8B**) and mesenchymal markers, such as CD29, CD44, and CD105. HLSC-EVs did not express hematopoietic (CD19, CD3, CD45, etc.), endothelial (CD31) and epithelial (CD24 and CD326) markers (**Figure 8B**). NTA showed the characteristic size distribution of a heterogeneous population of EVs (**Figure 8C**) and TEM analysis confirmed the presence of intact membrane (**Figure 8D**).

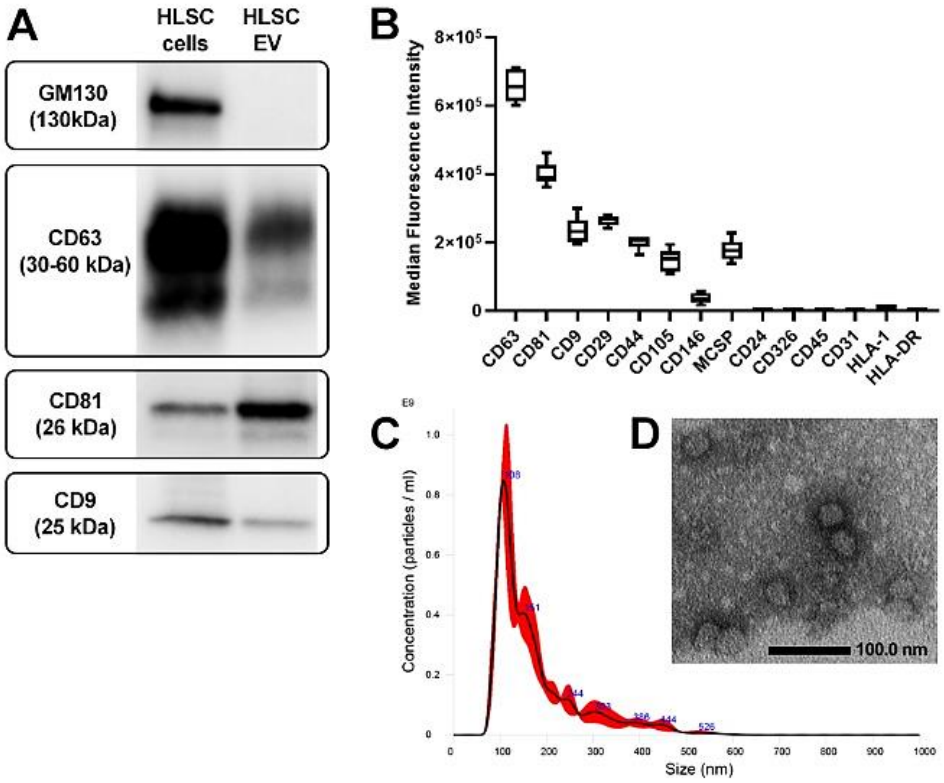

Figure 8. EVcharacterization. A) Representative Western Blot images of HLSCs and HLSC-EVs for the expression of the tetraspanins CD63, CD81 and CD9. As negative exosomal marker, the *cis*-Golgi protein GM130 is expressed only in cells. **B)** Cytofluorimetric analysis of surface proteins expressed on EVs. The graph shows the median allophycocyanin fluorescence values of 14 bead populations selected from 37 that can be screened using the MACSPlex Exosome Kit. **C)** Representative NTA chart illustrating concentration and size distribution of EVs. **D)** TEM figure of EVs contrasted with Nano-W™ and NanoVan™ (scale bar, 100 nm; magnification, 50,000×).

EV administration improves kidney function and morphology

We evaluated whether HLSC-EV administration may revert functional and histopathological alterations in PNx mice. EV treatment started 4 weeks after the nephrectomy, when the histopathological signs of CKD development were already evident. Three different doses of EVs were tested and mice were sacrificed 4 weeks after the first EV administration (**Figure 9A**). As shown in **Figure 9B and 9C**, EV treatment improved renal function: in fact, all tested EV doses significantly reduced creatinine plasma levels, compared to PNx mice treated with vehicle alone (**Figure 9B**). Instead, the reduction in BUN plasma levels reached statistical significance only in PNx mice treated with EV doses 1 and 2 (**Figure 9C**). Assessment of the histological alterations indicated that EV treatment with dose 1 significantly reduced interstitial fibrosis (**Figure 9D**) and glomerulosclerosis

(**Figure 9E**). Furthermore, EV dose 2 was able to significantly reduce interstitial fibrosis (**Figure 9D**), even to a lesser extent that dose 1, but did not ameliorate glomerular sclerosis (**Figure 9E**).

Figure 10 shows representative TEM pictures of SHAM, PNx mice treated with vehicle alone or with EV dose 1. Vehicle-treated PNx mice, compared with SHAM mice, showed tubular interstitial injuries characterized by increased matrix accumulation, monocyte infiltration with loss of peritubular capillaries, and glomerular alterations characterized by endothelial and epithelial injuries. The EV treatment markedly reduced the previously observed lesions. In particular, the enlargements and infiltrations of the interstitium, the loss of endothelium and the effacement of podocytes and glomeruli were reduced (**Figure 10**).

Another important feature of CKD is capillary rarefaction. To evaluate the possibility that EV treatment could improve capillary rarefaction, quantification of CD31 expression was performed in renal tissue of PNx mice. **Figure 9F** reports the effect of dose 1, as it was the dose that was functionally and histologically most effective in the kidney of PNx mice. EV administration significantly increased the percentage of CD31-positive cells in PNx mice, thus indicating that EVs could also counteract capillary rarefaction (**Figure 9F**).

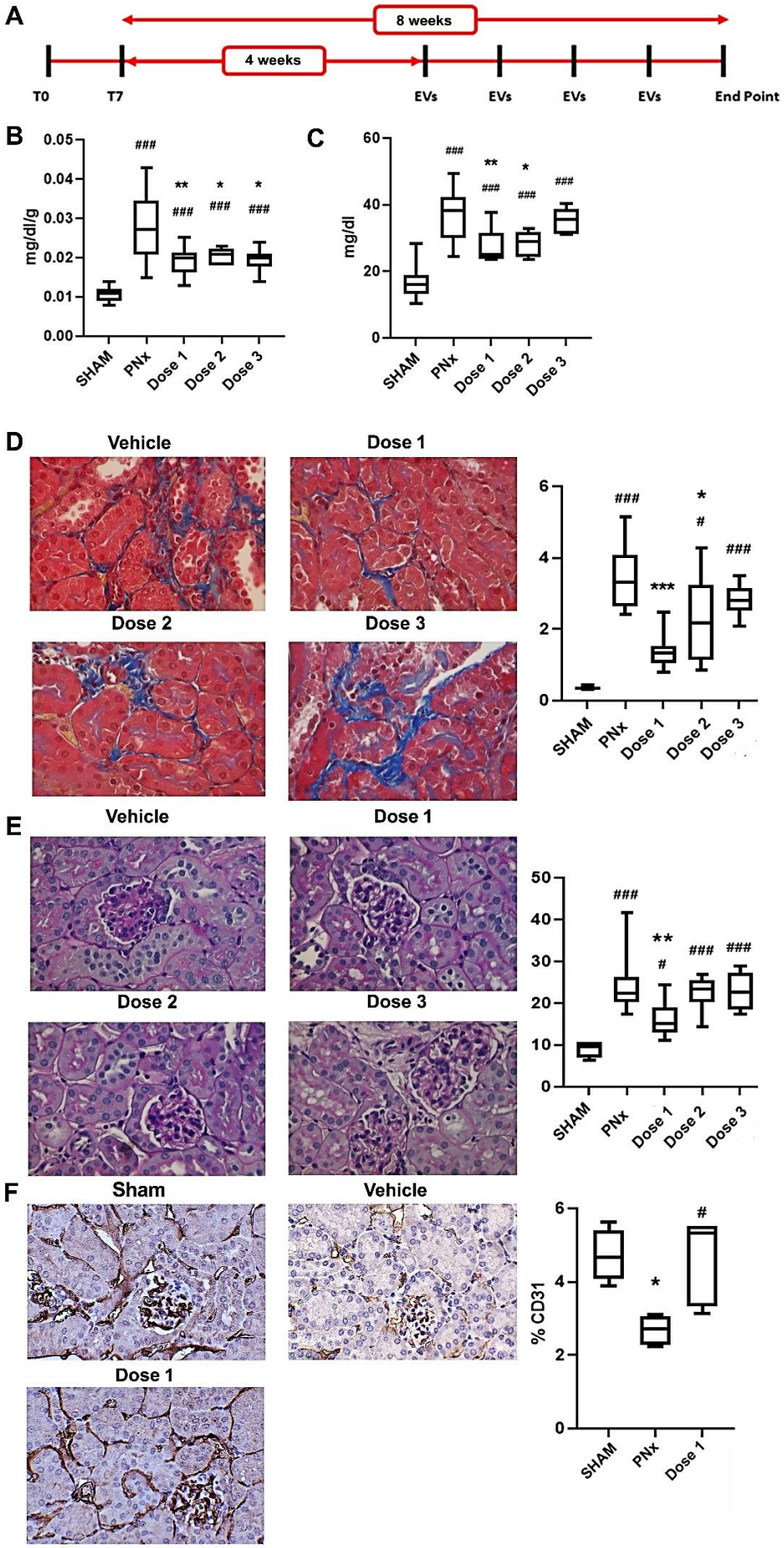
A
8 weeks
4 weeks
T0
T7
EVs
EVs
EVs
EVs
End Point
B
mg/dl/g
SHAM
PNx
Dose 1
Dose 2
Dose 3
C
mg/dl
D
Vehicle
Dose 1
Dose 2
Dose 3
E
Vehicle
Dose 1
Dose 2
Dose 3
F
Sham
Vehicle
Dose 1
% CD31

Figure 9. Effects of different EV-doses on renal function and morphology. A) Schematic representation of the experimental design to test EVs in CKD mice, showing the timings of surgeries (T0 and T7), of EV administrations and of sacrifice (end point). **B and C)** Evaluation of creatinine (**B**) and BUN (**C**) plasma levels of control SHAM mice (n=12) and of PNx mice sacrificed 8 weeks after the surgery treated with vehicle alone (n=8) or with different doses of EVs (n=10/dose 1 and n=6/doses 2 and 3). Results are shown as mean ± SD. Ordinary One Way ANOVA with Tukey's multiple comparison test was performed by Prism. For creatinine: $^{###}$ p ≤ 0.0001 PNx mice treated with vehicle or with different doses of EVs *versus* SHAM mice; **p ≤ 0.001 PNx mice treated with dose 1 and *p ≤ 0.02 PNx mice treated with dose 2 and 3 *versus* PNx mice treated with vehicle alone. For BUN: $^{###}$ p ≤ 0.0001 PNx mice treated with vehicle or with different doses of EVs *versus* SHAM mice; ** p ≤ 0.004 PNx mice treated with dose 1 and * p ≤ 0.03 PNx mice treated with dose 2 *versus* PNx mice treated with vehicle alone. **D)** Representative micrographs of Masson's trichrome stained renal sections of PNx mice treated with vehicle alone or with different doses of EVs. The blue stain represents collagen fibers considered a marker for renal interstitial fibrosis. Original magnification 400×. Bar chart on the right shows histological quantification of fibrosis of SHAM mice and of PNx mice treated with vehicle or with different EV doses, by multiphase image analysis of 10 fields per section. Results are shown as mean ± SD. Ordinary One Way ANOVA with Tukey's multiple comparisons test was performed by Prism. $^{###}$ p ≤ 0.0001 PNx mice treated with vehicle alone or with dose 3 versus SHAM mice and $^{#}$ p ≤ 0.008 PNx mice treated with dose 2 versus SHAM mice. *** p < 0.0001 PNx mice treated with dose 1 and * p ≤ 0.03 PNx mice treated with dose 2 *versus* PNx mice treated with vehicle alone. **E)** Representative micrographs of PAS-stained renal sections of PNx mice treated with vehicle alone or with different doses of EVs. Original magnification 400×. Bar chart on the right represents histological quantification of glomerular PAS+ deposition in SHAM mice, PNx mice treated with vehicle alone and PNx mice treated with different doses of EVs, by multiphase image analysis using ImageJ software on at least 15 glomeruli from each mouse. Results are shown as mean ± SD. Ordinary One Way ANOVA with Tukey's multiple comparisons test was performed by Prism. $^{###}$ p ≤ 0.0001 PNx mice treated with vehicle or with dose 2 and 3 and $^{#}$ p ≤ 0.001 PNx mice treated with dose 1 v*ersus* SHAM mice; ** p ≤ 0.002 PNx mice treated with dose 1 *versus* PNx mice treated with vehicle alone. **F)** Representative photographs of CD31 antibody-stained renal sections of SHAM mouse and of PNx mice treated with vehicle alone or with dose 1. In the graph on the right, CD31 expression was quantified in each experimental group. Statistical analysis was performed using the Ordinary One-way ANOVA test with Tukey's multiple comparisons test. * p ≤ 0.02 PNx mice treated with vehicle alone *versus* SHAM mice; # p ≤ 0.02 PNx treated with dose 1 *versus* PNx mice treated with vehicle alone.

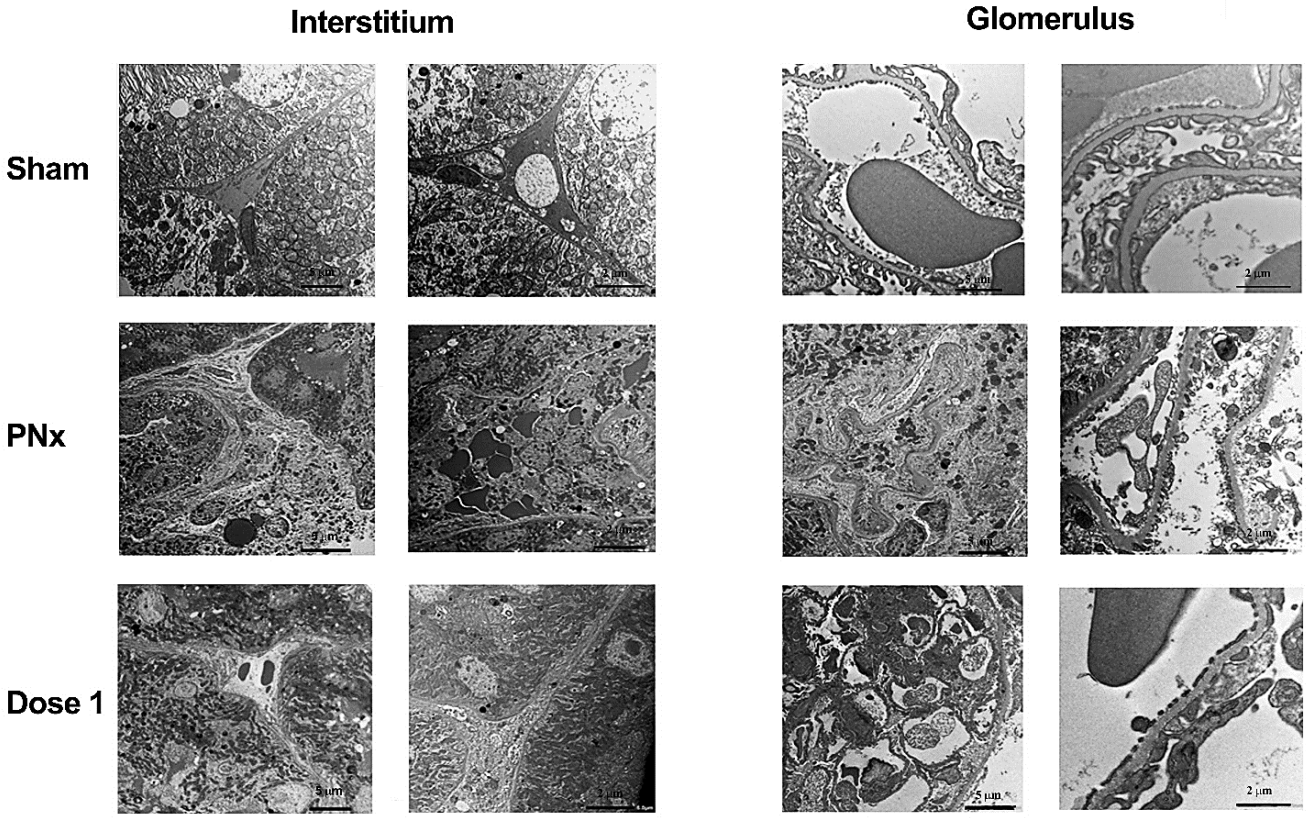

Figure 10. Ultrastructural changes of the interstitium and the glomeruli in PNx mice and the effects of EV treatment. TEM representative images of the interstitium and glomerulus of SHAM and PNx mice sacrificed 8 weeks after the nephrectomy and treated with vehicle alone or with EV dose 1. The bars indicate the magnification.

EV treatment modulates the expression of fibrosis and inflammation-related genes

To perform molecular analyses, RNA was isolated from renal tissues obtained from PNx mice treated with vehicle alone or with the effective EV doses, EV dose 1 and 2, which were the most effective at functional and histological level. PNx mice treated with EV doses 1 and 2 showed a significant reduction in alpha-SMA and COL1A1 gene expression levels, compared to PNx mice treated with vehicle alone (**Figure 11A**).

Gene expression level of TGF-beta was significantly downregulated only in PNx mice treated with dose 1 in respect to vehicle-treated PNx mice (**Figure 11A**).

Moreover, gene expression analysis of tumor necrosis factor-alpha (TNF-alpha) and interleukin (IL)-6 indicated an increase in the expression levels of these two pro-inflammatory markers in the renal tissue of PNx mice (**Figure 11B**). Only PNx mice treated with EV dose 1 showed a significant reduction in TNF-alpha expression level, compared to vehicle-treated PNx mice. In addition, a reduction in IL-6 gene expression level was observed in PNx mice treated with EV dose 1, although it did not reach statistical significance (**Figure 11B**).

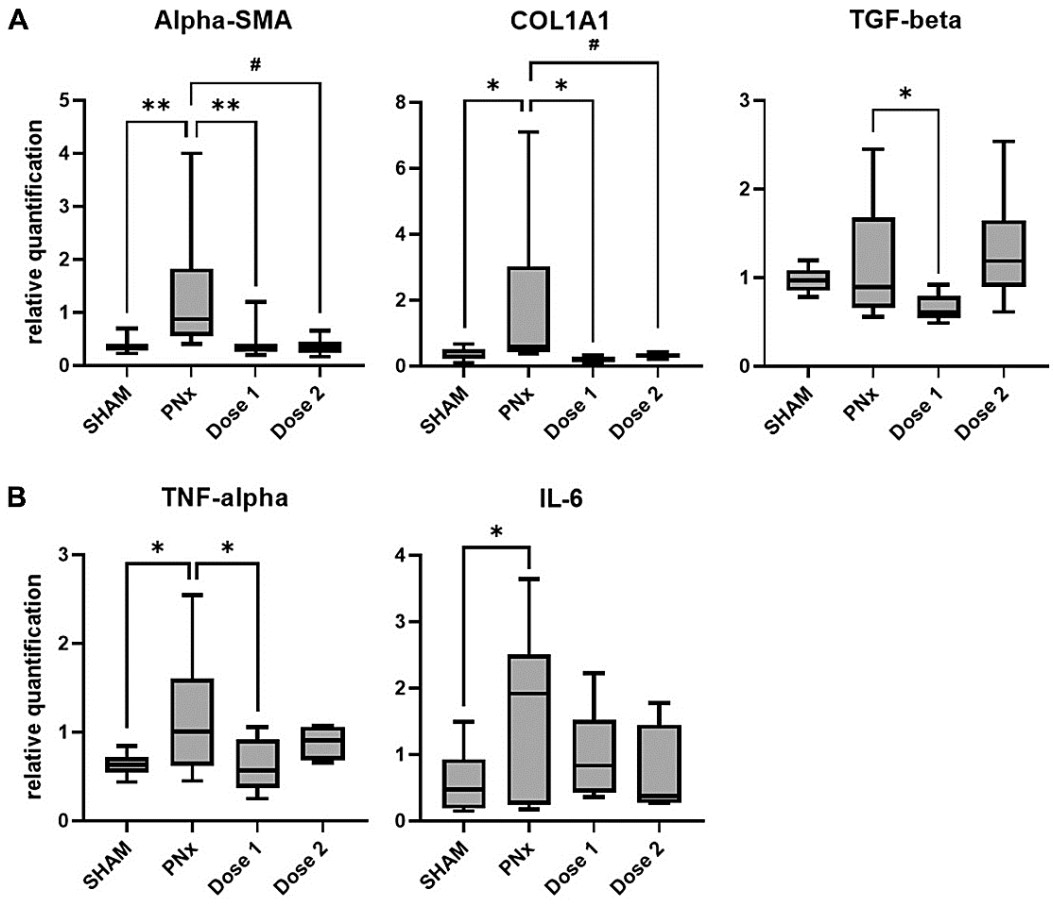

Figure 11. Expression levels of pro-fibrotic and pro-inflammatory genes in PNx mice treated with EVs or with vehicle alone. A) Gene expression levels of the fibrosis-related markers Alpha-SMA, COL1A1 and TGF-beta in PNx mice treated with EV doses 1 (n=10) and 2 (n=6), or with vehicle alone (n=10), and SHAM mice (n=10). Data are normalized to GAPDH. Mean ± SD was calculated by comparing the gene expression levels of each experimental group with those of the PNx group treated with vehicle alone. Statistical analysis was performed using the Two-way ANOVA test with Dunnett's multiple comparison test. Alpha-SMA: **$p \leq 0.002$ PNx mice treated with vehicle *versus* SHAM mice and PNx mice treated with dose 1 *versus* PNx mice treated with vehicle alone; $^{\#}p \leq 0.01$ PNx mice treated with dose 2 *versus* PNx mice treated with vehicle. COL1A1: *$p \leq 0.01$ PNx mice treated with vehicle alone *versus* SHAM mice and PNx treated with dose 1 *versus* PNx mice treated with vehicle; $^{\#}p \leq 0.05$ PNx mice treated with dose 2 *versus* PNx mice treated with vehicle. TGF-beta: *$p \leq 0.05$ PNx mice treated with dose 1 *versus* PNx mice treated with vehicle. **B)** Gene expression levels of the inflammatory markers TNF-alpha and IL-6 in PNx mice treated with EV dose 1 (n=10) and 2 (n=6), or with vehicle alone (n=10) and SHAM mice (n=10). Data are normalized to GAPDH. Mean ± SD was calculated by comparing the gene expression levels of each experimental group with those of the PNx group treated with vehicle alone. Statistical analysis was performed using the Two-way ANOVA test with Dunnett's multiple comparison test. TNF-alpha: *$p \leq 0.02$ PNx mice treated with vehicle *versus* SHAM mice and PNx mice treated with dose 1 *versus* PNx mice treated with vehicle; IL-6: *$p \leq 0.02$ PNx mice treated with vehicle *versus* SHAM mice.

EV treatment ameliorates cardiac function and morphology

The effects of HLSC-EV administration were also evaluated on cardiac function by echocardiographic analysis. Compared to SHAM mice, PNx mice injected with vehicle alone showed a reduction in left

ventricular (LV) mass and myocardial wall thickness, in particular at the level of the interventricular septum in diastole (IVSd), and of the left ventricular internal diameter in systole and diastole (LVIDs-LVIDd) (**Figure 12A**). Furthermore, a reduction in mitral valve (MV) deceleration time, a hallmark of diastolic dysfunction, was observed. In PNx mice treated with EV dose 1 these same parameters, such as the LV mass, IVS, LVID and MV deceleration time, showed a trend towards amelioration (**Figure 12A**). Despite this, the observed differences among PNx mice treated with EV dose 1 and PNx mice treated with vehicle alone reached the statistical significance only for LVIDs. Interestingly, for the other parameters (MV deceleration time, IVSs and LVIDd) no statistically significant differences were detected between PNx mice treated with EV dose 1 and SHAM mice.

Interstitial fibrosis is considered a key hallmark of diastolic dysfunction. Histopathological analysis revealed the presence of a mild-to-moderate focal or multifocal interstitial fibrosis located in the sub-endocardial area, in all PNx mice of the set-up group (sacrificed 4 and 8 weeks after the nephrectomy) and in 6 out of 7 vehicle-treated PNx mice (sacrificed 8 weeks after the nephrectomy). Only 1 out of 10 PNx mice treated with EV dose 1 and 1 out of 6 PNx mice injected with EV doses 2 and 3 exhibited interstitial fibrosis (**Table 2** and **Figure 12B**). None of the mice presented cardiomyocytes atrophy, inflammation and necrosis, regardless of their treatment group. These data indicate that the different tested EV doses had an anti-fibrotic effect on cardiac tissue, at least at histological level.

Molecular analyses were also performed on the cardiac tissues of PNx mice treated with the effective EV doses or with vehicle alone. However, no statistically significant differences were observed between EV-treated PNx mice and vehicle-treated PNx mice (data not shown).

Table 2. Histopathological results of cardiac tissues analyses.

Group	Fibrosis				
	Type	Number of cases with increased fibrosis	Overall Grade	Location	Distribution
SHAM	Absent	0/8	None	n.a.	n.a.
PNx month 1	Interstitial	3/3	Mild	Sub-endocardium	Focal
PNx month 2	Interstitial	5/5	Mild	Sub-endocardium	Multifocal
PNx + vehicle	Interstitial	6/7	Mild	Sub-endocardium	Focal
PNx + EV Dose 1	Interstitial	1/10	Mild	Sub-endocardium	Focal
PNx + EV Dose 2	Interstitial	1/6	Mild	Sub-endocardium	Focal
PNx + EV Dose 3	Interstitial	1/6	Moderate	Sub-endocardium	Focal

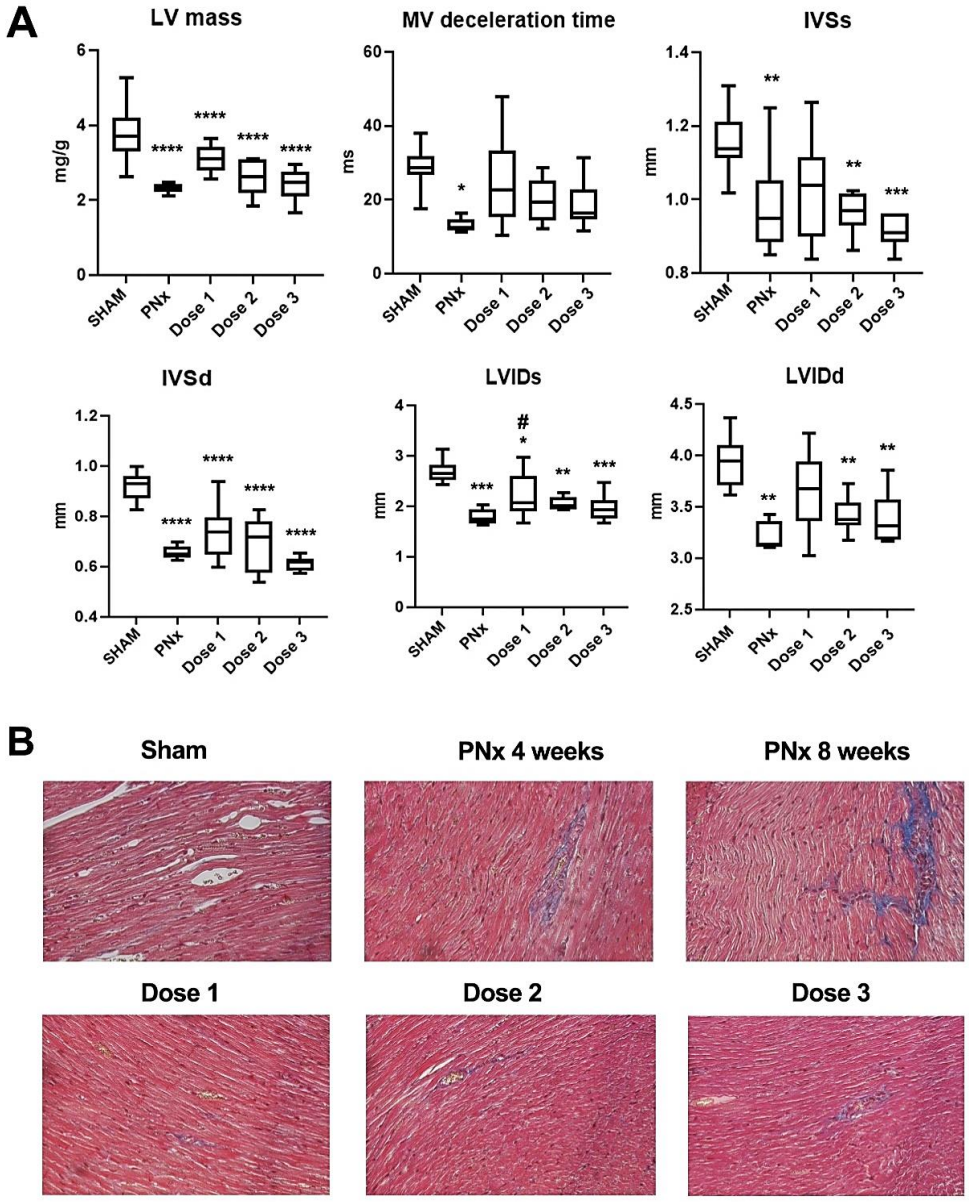

Figure 12. Effects of different EV doses on cardiac function and morphology. A) Bar charts showing the results of echocardiographic analysis of SHAM mice and PNx mice treated with vehicle alone or with different EV doses. LV mass, left ventricle mass; MV deceleration time, mitral valve deceleration time; IVDs and IVDd, interventricular septum thickness in systole (s) and diastole (d); LVIDs and LVIDd, left ventricle internal diameter in systole (s) and diastole (d). Results are shown as mean ± SD. Ordinary One Way ANOVA with Tukey's multiple comparisons test was performed by Prism. LV mass normalized to body weight: ****$p \leq 0.0001$ PNx mice treated with vehicle or with different EV dose *versus* SHAM mice; MV deceleration time: *$p \leq 0.01$ PNx mice treated with vehicle *versus* SHAM mice; IVSs: **$p \leq 0.05$ PNx mice treated with vehicle or with dose 2 *versus* SHAM mice and ***$p \leq 0.0005$ PNx mice treated with dose 3 *versus* SHAM mice; IVSd: ****$p \leq 0.0001$ PNx mice treated with vehicle or with different EV doses *versus* SHAM mice; LVIDs: *$p \leq 0.05$ PNx mice treated with dose 1 *versus* SHAM mice, **$p \leq 0.002$ PNx mice treated with dose 2 *versus* SHAM mice, ***$p \leq 0.0003$ PNx mice treated with vehicle or with dose 3 *versus* SHAM mice and # $p \leq 0.05$ PNx mice treated with dose 1 *versus* PNx mice treated with vehicle; LVIDd: **$p \leq 0.005$ PNx mice treated with vehicle or with dose 2 and 3 *versus* SHAM mice. **B)** Micrographs of Masson's trichrome stained cardiac sections of representative SHAM mouse, PNx mouse sacrificed 4 weeks after the nephrectomy and PNx mice sacrificed 8 weeks after the nephrectomy and treated with vehicle alone or with different EV doses. The blue stain represents collagen fibers considered a marker of fibrosis. Original magnification 200×.

Protease content of EVs and its implication in their anti-fibrotic effect *in vivo*

Proteomic analyses using an antibody-based array approach showed an EV-profile related to the ECM remodeling capacity (**Figure 13A**). In particular, the screening of 35 proteases on cells and EV lysates demonstrated that, compared to the cells of origin, EVs are enriched in MMP1 and 2. Furthermore, in both cells and EVs other proteases with ECM degradation activities were detected, such as ADAM9, ADAM with thrombospondin motifs 1 (ADAMTS1), dipeptidyl peptidase-4 (DPPIV, also known as CD26) and uPA (**Figure 13B**).

Protein expression of ADAM9, MMP1 and 2, DPPIV and uPA was also evaluated by Western Blot analyses in cells, EVs isolated by ultracentrifugation (UC-EVs) and EVs isolated by floating (FL-EVs), since the presence of these proteases could be ascribed to the method used to obtain the EVs, Western Blot analyses demonstrated that FL-EVs still contain MMP1 and 2, ADAM9 and DPPIV, indicating that these proteases are shuttled by EVs and not only co-precipitated during the ultracentrifugation procedure (**Figure 13C**).

To better investigate the involvement of the proteases transported by EVs in their *in vivo* anti-fibrotic effect in CKD, a neutralizing anti-human MMP1 antibody was used to treat EVs before their

administration in PNx mice. Treatment of EVs with neutralizing anti-human MMP1 antibody decreased their *in vivo* beneficial effect (**Figure 13D and 13E**). In particular, in PNx mice that received EVs pre-treated with the MMP1-blocking antibody, a decreased capacity of EVs to reduce renal fibrosis was observed at histological level (**Figure 13D and 13E**). These data indicate a possible role of EV-transported MMP1 in their anti-fibrotic activity on renal tissue in PNx murine model. Pre-treatment of EVs with anti-human MMP1 antibody did not influence their anti-fibrotic effect on cardiac tissue (data not shown), suggesting the presence of different EV mechanisms of action in different target tissues.

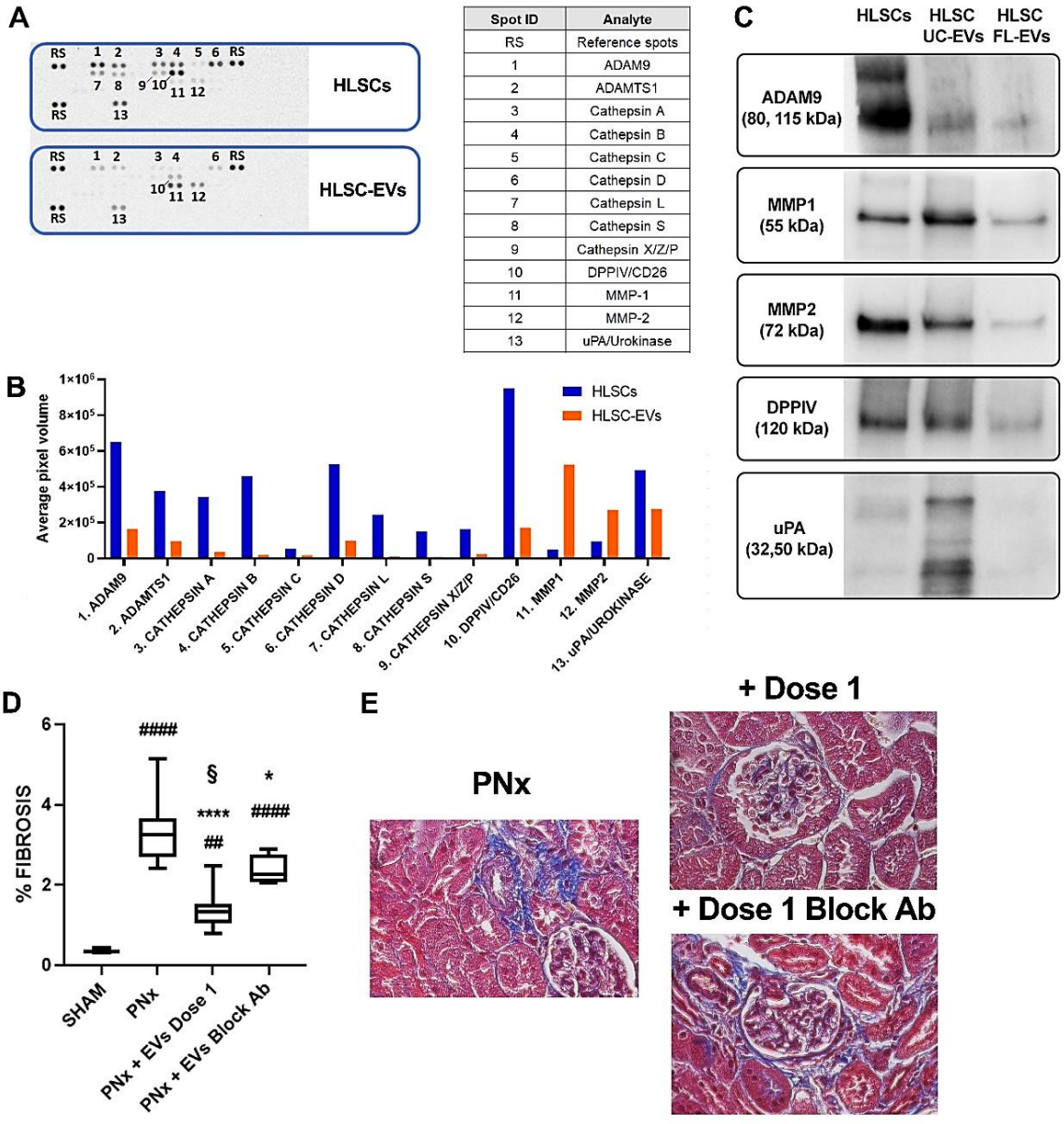

Spot ID	Analyte
RS	Reference spots
1	ADAM9
2	ADAMTS1
3	Cathepsin A
4	Cathepsin B
5	Cathepsin C
6	Cathepsin D
7	Cathepsin L
8	Cathepsin S
9	Cathepsin X/Z/P
10	DPPIV/CD26
11	MMP-1
12	MMP-2
13	uPA/Urokinase

Figure 13. Protease expression profile. A) Representative image of the results of Proteome Profiler™ Human Protease Array, comparing the expression of 35 human proteases among HLSC and HLSC-EV protein lysate. The top 13 proteases expressed in cells and EVs are listed in the table on the right. **B)** Histogram representing the average signal (pixel density of the spots) of the 13 proteases expressed in cell protein lysate (blue bars) and in EV lysate (orange bars). **C)** Representative image of the results of Western Blot analyses of 5 proteases expressed in protein lysate of cells and EVs purified by ultracentrifugation (UC-EVs) and EVs purified by floating (FL-EVs). **D)** Histological quantification of fibrosis in SHAM mice (n=7), PNx mice treated with vehicle alone (n=5) and PNx mice injected with EV dose 1 pre-treated or not with blocking antibody (n=6/group). Renal fibrosis was quantified by measuring collagenous fibrotic areas stained in blue in 10 random renal fields/section, from images acquired at a magnification of 400×. Results are shown as mean ± SD. Ordinary One Way ANOVA with Tukey's multiple comparisons test was performed by Prism. $^{\#\#\#\#}p \leq 0.0001$ PNx mice treated with vehicle alone or with EV pre-treated with blocking antibody and $^{\#\#}p \leq 0.003$ PNx mice treated with EVs *versus* SHAM mice; $^{****}p \leq 0.0001$ PNx mice treated with EVs and $^{*}p \leq 0.03$ PNx mice treated with EVs pre-treated with blocking antibody *versus* PNx mice treated with vehicle alone; $^{\S}p \leq 0.04$ PNx mice treated with EVs *versus* PNx mice treated with EVs pre-treated with blocking antibody. **E)** Representative micrographs of Masson's trichrome stained renal sections of PNx mice treated with vehicle alone or EV dose 1 pre-treated or not with specific blocking antibody. The blue stain represents collagen fibers considered a marker for renal interstitial fibrosis. Original magnification 400×.

Discussion

Rat and murine 5/6th PNx models recapitulate the main features of CKD development after loss of kidney mass and function in human patients (Tan *et al.*, 2019). In this model, it has been demonstrated that vesicles isolated from bone marrow (BM)-derived MSCs protected the kidney from renal injury (He *et al.*, 2012). Like BM-MSCs, BM-MSC-EVs reduced proteinuria, interstitial fibrosis, lymphocyte infiltrates and tubular atrophy (He *et al.*, 2012). Similar results were obtained in a rat 5/6th ablation model, where BM-MSC-EVs protected against kidney injury by up-regulating the expression and the activity of Klotho, a reno-protective molecule (Wan *et al.*, 2022).

The conventional ablation model may cause post-operative bleeding, infection, and mortality (Tan *et al.*, 2019). As previously described, the 5/6th PNx model with pole ligation represents a valuable surgical alternative, and for these reasons, we set up the 5/6th PNx ligation model in immunodeficient SCID male mice.

The analysis of renal function and histology indicated that the development of interstitial fibrosis and glomerulosclerosis was already evident 4 weeks after the nephrectomy and the injury further increased in mice sacrificed at week 8 post-nephrectomy. This trend was confirmed by the molecular analyses of the expression of specific markers of fibrosis in the renal tissues. Moreover, signs of diastolic dysfunction and cardiac fibrosis have been observed in SCID mice subjected to PNx procedures.

In this murine model, we tested the therapeutic effects of HLSC-EVs on the development of CKD, cardiac fibrosis, and diastolic dysfunction. Different doses of HLSC-EVs have been weekly and intravenously administered to PNx mice, starting at week 4 after the nephrectomy, when signs of renal and cardiac chronic injuries were already evident.

Our results indicate that multiple HLSC-EV administrations exerted beneficial effects on renal function and morphology, both at the tubular and glomerular levels. Furthermore, the results obtained on cardiac tissue indicate for the first time that the EV treatment also exerted a beneficial effect on cardiac fibrosis and diastolic dysfunction. These data showed that HLSC-EVs could have favorable

effects in different organs at both functional and histological levels, as previously reported for EVs isolated from adipose-derived MSCs (Lindoso *et al.*, 2020).

In renal tissues of PNx mice treated with HLSC-EVs, we observed down-regulation of the gene expression levels of specific markers of fibrosis such as alpha-SMA, COL1A1 and TGF-beta. Similar results have been previously obtained by injecting HLSC-EVs in mouse models of AA-induced kidney fibrosis (Kholia *et al.*, 2018) and IRI-induced CKD (Bruno *et al.*, 2022).

Several studies have shown the importance of microRNAs (miRNAs) shuttled by HLSC-EVs in their anti-fibrotic and anti-inflammatory effects, and the relevance of the miRNAs shuttled by HLSC-EVs was shown in a murine model of diabetic nephropathy (Grange, Tritta *et al.*, 2019). The miRNA cargo of HLSC-EV includes miR-17-5p, miR-106a-5p and miR-155-5p, which are involved in the regulation of different molecular pathways, such as adhesion molecule-cadherin signaling pathways known to contribute to fibrosis progression (Grange, Tritta *et al.*, 2019). Moreover, HLSC-EVs shuttle miR-146a, which contributes to the inhibition of inflammation in diabetic nephropathy-induced CKD (Grange, Tritta *et al.*, 2019) (Bhatt *et al.*, 2016) and also to the *in vitro* HLSC-EV anti-fibrotic activity (Chiabotto *et al.*, 2021).

The biological activity of HLSC-EVs is also influenced by their protein content. In fact, our previous proteomic analysis revealed the presence of several anti-inflammatory proteins, such as enzymes, tyrosine kinase receptors and transcription factors in the HLSC-EV cargo (Bruno *et al.*, 2020).

Most of them are involved in IL-10, p53 or Phosphoinositide 3 Kinase (PI3K) signaling pathways, thus contributing to the HLSC-EV anti-fibrotic and anti-inflammatory activity.

To better understand the mechanisms associated with the EV beneficial effects, we analyzed the protease content of our vesicle population. Protein array and Western Blot analyses showed that HLSC-EVs shuttle MMP1, MMP2 and other proteases with ECM degradation capacity. Through mass spectrometry and antibody array, it has been reported that exosomes purified from embryonic stem cell (ESC)-derived MSCs contain MMP1, MMP3, MMP10, ADAM9 and ADAMTS12 (Lai *et al.*,

2012). However, the possible involvement of these proteases in the *in vivo* beneficial effects of ESC-MSC-EVs has not been evaluated. Instead, the contribution of protein components of 20S proteasome to the cardioprotective activity of ESC-MSC-EVs, through proteolytic degradation of misfolded proteins, has been demonstrated in ischemic cardiac tissue (Lai *et al.*, 2012).

Here, we report the possible contribution of proteases associated with HLSC-EVs to their anti-fibrotic activities on renal tissue. By administering HLSC-EVs pre-treated with specific human anti-MMP1 blocking antibody to PNx mice, we observed a reduced capacity of these EVs to counteract renal fibrosis development, indicating a possible implication of MMP1 in the therapeutic potential of HLSC-EVs.

Recently, the anti-fibrotic activity of MMP1 decorated polymersomes (MMPsomes) has been reported in an *in vivo* model of hepatic fibrosis (Geervliet *et al.*, 2021). This innovative approach of MMP1 delivery, using surface-decorated synthetic vesicles, seems to be efficient in reducing collagen deposition *in vivo* (Geervliet *et al.*, 2021). HLSC-EVs naturally transport MMP1 and other ECM-degrading proteases. Therefore, collagen degradation is a candidate mechanism underlying the anti-fibrotic effect of HLSC-EVs that mediates the reduction of tissue fibrosis through EV-associated proteases and other well-known molecular components (e.g. miRNA, mRNA, etc...).

Conclusions

In conclusion, our results show that, in PNx mice with established CKD and cardiac dysfunction, multiple injections of different doses of HLSC-EVs can effectively improve renal and cardiac function and morphology, mainly through the reduction of tissue fibrosis.

Moreover, at least in renal tissue, we demonstrated that HLSC-EV-shuttled proteases could be involved in their *in vivo* anti-fibrotic activity. In particular, a possible involvement of EV-mediated delivery of MMP1 seems to be implicated, since the specific blocking of MMP1 decreases the EV ability to attenuate fibrosis in renal tissue of PNx mice.

Further studies will be necessary to better elucidate the mechanism of action of EV-shuttled proteases and their implications for the EV *in vivo* anti-fibrotic activity.

References

Abecassis, M., Bartlett, S. T., Collins, A. J., Davis, C. L., Delmonico, F. L., Friedewald, J. J., et al. (2008). Kidney transplantation as primary therapy for end-stage renal disease: A National Kidney Foundation/Kidney Disease Outcomes Quality Initiative (NKF/KDOQI^{TM}) conference. *Clin J Am Soc Nephrol* 3, 471–480. doi: 10.2215/CJN.05021107.

Andreu, Z., Yáñez-Mó, M. (2014). Tetraspanins in extracellular vesicle formation and function', *Frontiers in Imm* 5, 1–12. doi: 10.3389/fimmu.2014.00442.

Bhatt, K., Lanting, L. L., Jia, Y., Yadav, S., Reddy, M. A., Magilnick, N., et al. (2016). Anti-inflammatory role of MicroRNA-146a in the pathogenesis of diabetic nephropathy. *J Am Soc Nephrol* 27, 2277–2288. doi: 10.1681/ASN.2015010111.

Birtwistle, L., Chen, X.-M., and Pollock, C. (2021). Mesenchymal stem cell-derived extracellular vesicles to the rescue of renal injury. *Int J Mol Sci* 22, 6596. doi: 10.3390/ijms22126596.

Bruno, S., Grange, C., Deregibus, M. C., Calogero, R. A., Saviozzi, S., Collino, F., et al. (2009). Mesenchymal stem cell-derived microvesicles protect against acute tubular injury. *J Am Soc Nephrol* 20, 1053–1067. doi: 10.1681/ASN.2008070798.

Bruno, S., Grange, C., Tapparo, M., Pasquino, C., et al. (2016). Human Liver Stem Cells Suppress T-Cell Proliferation, NK Activity, and Dendritic Cell Differentiation. *Hindawi*. doi: 10.1155/2016/8468549.

Bruno, S., Herrera Sanchez, M. B., Pasquino, C., Tapparo, M., Cedrino, M., Tetta, C., et al. (2019). Human Liver-Derived Stem Cells Improve Fibrosis and Inflammation Associated with Nonalcoholic Steatohepatitis. *Stem Cells Int*, 6351091. doi: 10.1155/2019/6351091.

Bruno, S., Pasquino, C., Herrera Sanchez, M. B., Tapparo, M., Figliolini, F., Grange, C., et al. (2020). HLSC-Derived Extracellular Vesicles Attenuate Liver Fibrosis and Inflammation in a Murine Model of Non-alcoholic Steatohepatitis. *Mol Ther* 28, 479–489. doi: 10.1016/j.ymthe.2019.10.016.

Bruno, S., Herrera Sanchez, M. B., Chiabotto, G., Fonsato, V., Navarro-Tableros, V., Pasquino, C., et al. (2021). Human Liver Stem Cells: A Liver-Derived Mesenchymal Stromal Cell-Like Population With Pro-regenerative Properties. *Front Cell Dev Biol* 9, 1–14. doi: 10.3389/fcell.2021.644088.

Bruno, S., Chiabotto, G., Cedrino, M., Ceccotti, E., Pasquino, C., De Rosa, S., et al. (2022). Extracellular Vesicles Derived from Human Liver Stem Cells Attenuate Chronic Kidney Disease Development in an In Vivo Experimental Model of Renal Ischemia and Reperfusion Injury. *Int J Mol Sci* 23, 1485. doi: 10.3390/ijms23031485.

Chen, C., Xie, C., Wu, H., et al. (2021). Uraemic Cardiomyopathy in Different Mouse Models. *Front in Med* 8, 1–12. doi: 10.3389/fmed.2021.690517.

Chiabotto, G., Ceccotti, E., Tapparo, M., Camussi, G., Bruno, S. (2021). Human Liver Stem Cell-Derived Extracellular Vesicles Target Hepatic Stellate Cells and Attenuate Their Pro-fibrotic Phenotype. *Front Cell Dev Biol* 9, 777462. doi: 10.3389/fcell.2021.777462.

Deregibus, M. C., Figliolini, F., D'Antico, S., Manzini, P. M., Pasquino, C., De Lena, M., et al. (2016). Charge-based precipitation of extracellular vesicles', *Int J Mol Med* 38, 1359–1366. doi: 10.3892/ijmm.2016.2759.

Gay-Jordi, G., Guash, E., Benito, B., Brugada, J., Nattel, S., Mont, L., et al. (2013). Losartan Prevents Heart Fibrosis Induced by Long-Term Intensive Exercise in an Animal Model. *PLoS ONE* 8, 1–8. doi: 10.1371/journal.pone.0055427.

Geervliet, E., Moreno, S., Baiamonte, L., Booijink, R., Boye, S., Wang, P., et al. (2021). Matrix metalloproteinase-1 decorated polymersomes, a surface-active extracellular matrix therapeutic, potentiates collagen degradation and attenuates early liver fibrosis. *J Control Release* 332, 594–607. doi: 10.1016/j.jconrel.2021.03.016.

Grange, C., Tritta, S., Tapparo, M., Cedrino, M., Tetta, C., Camussi, G., et al. (2019). Stem cell-derived extracellular vesicles inhibit and revert fibrosis progression in a mouse model of diabetic nephropathy. *Sci Rep* 9, 4468. doi: 10.1038/s41598-019-41100-9.

Grange, C., Skovronova, R., Marabese, F., Bussolati, B. (2019). Stem Cell-Derived Extracellular Vesicles and Kidney Regeneration. *Cells* 8, 1–13. doi: 10.3390/cells8101240.

Gürtl, B., Kratky, D., Guelly, C., Zhang, L., Gorkiewicz, G., Das, S. K., et al. (2009). Apoptosis and fibrosis are early features of heart failure in an animal model of metabolic cardiomyopathy. *Int J Exp Pathol* 90, 338–346. doi: 10.1111/j.1365-2613.2009.00647.x.

He, J., Wang, Y., Sun, S., Yu, M., Wang, C., Pei, X., et al. (2012). Bone marrow stem cells-derived microvesicles protect against renal injury in the mouse remnant kidney model. *Nephrol (Carlton)* 17, 493–500. doi: 10.1111/j.1440-1797.2012.01589.x.

Herrera, M. B., Bruno, S., Buttiglieri, S., Tetta, C., Gatti, S., Deregibus, M. C., et al. (2006). Isolation and Characterization of a Stem Cell Population from Adult Human Liver. *Stem Cells* 24, 2840–2850. doi: 10.1634/stemcells.2006-0114.

Herrera, M. B., Bruno, S., Grange, C., Tapparo, M., et al. (2014). Human liver stem cells and derived extracellular vesicles improve recovery in a murine model of acute kidney injury. *Stem Cell Res Ther* 5, 1–11. doi: 10.1186/scrt514.

Herrmann, I. K., Wood, M. J. A., Fuhrmann, G. (2021). Extracellular vesicles as a next-generation drug delivery platform. *Nat Nanotechnol* 16, 748–759. doi: 10.1038/s41565-021-00931-2.

Ishibashi-Ueda, H., Matsuyama, T.-A., Ohta-Ogo, K., and Ikeda, Y. (2017). Significance and value of endomyocardial biopsy based on our own experience. *Circ J* 81, 417–426. doi: 10.1253/circj.CJ-16-0927.

Jokinen, M. P., Lieuallen, W. G., Johnson, C. L., Dunnick, J., Nyska, A. (2005). Characterization of spontaneous and chemically induced cardiac lesions in rodent model systems: The National Toxicology Program experience. *Cardiovasc Toxicol* 5, 227–244. doi: 10.1385/CT:5:2:227.

Jokinen, M. P., Lieuallen, W. G., Boyle, M. C., Johnson, C. L., Malarkey, D. E., Nyska, A. (2011). Morphologic aspects of rodent cardiotoxicity in a retrospective evaluation of national toxicology program studies. *Toxicol Pathol* 39, 850–860. doi: 10.1177/0192623311413788.

Kholia, S., Herrera Sanchez, M. B., Cedrino, M., Papadimitriou, E., Tapparo, M., Deregibus, M. C., et al. (2018). Human liver stem cell-derived extracellular vesicles prevent aristolochic acid-induced kidney fibrosis. *Front Immunol* 9, 1639. doi: 10.3389/fimmu.2018.01639.

Koliha, N., Wiencek, Y., Heider, U., Jüngst, C., Kladt, N., Krauthäuser, S., et al. (2016). A novel multiplex bead-based platform highlights the diversity of extracellular vesicles. *J Extracell Vesicles* 5, 29975. doi: 10.3402/jev.v5.29975.

Kovesdy, C. P. (2022). Epidemiology of chronic kidney disease: an update 2022. *Kidney Int Suppl* 12, 7–11. doi: 10.1016/j.kisu.2021.11.003.

Kowal, J., Arras, G., Colombo, M., Jouve, M., Morath, J. P., Primdal-Bengtson, B., et al. (2016). Proteomic comparison defines novel markers to characterize heterogeneous populations of extracellular vesicle subtypes. *Proc Nat Acad Sci USA* 113, E968–E977. doi: 10.1073/pnas.1521230113.

Lai, R. C., Tan, S. S., Teh, B. J., Sze, S. K., Arslan, F., de Kleijn, D. P., et al. (2012). Proteolytic Potential of the MSC Exosome Proteome: Implications for an Exosome-Mediated Delivery of Therapeutic Proteasome. *Int J Proteomics*, 971907. doi: 10.1155/2012/971907.

Leaf, I. A., Duffield, J. S. (2017). What can target kidney fibrosis?. *Nephrology Dialysis Transplantation* 32, I89–I97. doi: 10.1093/ndt/gfw388.

Lindoso, R. S., Lopes, J. A., Binato, R., Abdelhay, E., Takiya, C. M., Miranda, K. R., et al (2020). Adipose Mesenchymal Cells-Derived EVs Alleviate DOCA-Salt-Induced Hypertension by Promoting Cardio-Renal Protection. *Mol Ther Methods Clin Dev* 16, 63–77. doi: 10.1016/j.omtm.2019.11.002.

Lu, Y., Wang, L., Zhang, M., Chen, Z. (2022). Mesenchymal Stem Cell-Derived Small Extracellular Vesicles : A Novel Approach for Kidney Disease Treatment. Int J Nanomedicine 17, 3603–3618. doi: 10.2147/IJN.S372254.

Merimi, M., El-Majzoub, R., Lagneaux, L., Moussa Agha, D., Bouhtit, F., Meuleman, N., et al. (2021). The Therapeutic Potential of Mesenchymal Stromal Cells for Regenerative Medicine: Current Knowledge and Future Understandings. *Front Cell Dev Biol* 9. doi: 10.3389/fcell.2021.661532

Monsel, A., Ying-gang, Z., Gennai, S., Hao, Q., Hu, S., Rouby, J. J., *et al.* (2015). Therapeutic effects of human mesenchymal stem cell-derived microvesicles in severe pneumonia in mice. *Am J Respir Crit Care Med* 192, 324–336. doi: 10.1164/rccm.201410-1765OC.

Niculae, A., Gherghina, M.E., Peride, I., Tiglis, M., Nechita, A.M., Checherita, I.A. (2023). Pathway from Acute Kidney Injury to Chronic Kidney Disease: Molecules Involved in Renal Fibrosis. *Int J Mol Sci* 24, 14019. doi: 10.3390/ijms241814019.

Picinich, S. C., Mishra, P. J., Mishra, P. J., Glod, J., Banerjee, D. (2007). The therapeutic potential of mesenchymal stem cells. *Expert Opin. Biol. Ther* 54, 965–973. doi: 10.1186/s40659-021-00366-y.

Ranghino, A., Bruno, S., Bussolati, B., Moggio, A., Dimuccio, V., Tapparo, M., et al. (2017). The effects of glomerular and tubular renal progenitors and derived extracellular vesicles on recovery from acute kidney injury. *Stem Cell Res Ther* 8, 1–15. doi: 10.1186/s13287-017-0478-5.

Serra, R. (2020). Matrix Metalloproteinases in Health and Disease. *Biom* 10, 9–11. doi: 10.3390/biom12091190.

Shimoda, M., Khokha, R. (2017). Metalloproteinases in extracellular vesicles. *Biochim Biophys Acta Mol Cell Res* 1864, 1989–2000. doi: 10.1016/j.bbamcr.2017.05.027.

Spada, M., Porta, F., Righi, D., Gazzera, C., Tandoi, F., Ferrero, I., et al. (2020). Intrahepatic Administration of Human Liver Stem Cells in Infants with Inherited Neonatal-Onset Hyperammonemia: A Phase I Study. *Stem Cell Rev Rep* 16, 186–197. doi: 10.1007/s12015-019-09925-z.

Tan, R.-Z., Zhong, X., Li, J.-C., Zhang, Y.-W., Yan, Y., Liao, Y., et al. (2019). An optimized 5/6 nephrectomy mouse model based on unilateral kidney ligation and its application in renal fibrosis research. *Ren Fail* 41, 555–566. doi: 10.1080/0886022X.2019.1627220.

Trohatou, O., Roubelakis, M. G. (2017). Mesenchymal Stem/Stromal Cells in Regenerative Medicine: Past, Present, and Future. *Cell Reprogram* 19, 217–224. doi: 10.1089/cell.2016.0062.

Visse, R., Nagase, H. (2003). Matrix metalloproteinases and tissue inhibitors of metalloproteinases: Structure, function, and biochemistry. *Circ Res* 92, 827–839. doi: 10.1161/01.RES.0000070112.80711.3D.

Wan, F., Yang, R. C., Tang, Y. W., et al (2022). BMSC-derived exosomes protect against kidney injury through regulating klotho in 5/6 nephrectomy rats. *Euro J Med Res* 27, 1–9. doi: 10.1186/s40001-022-00742-8.

Wang, X., Chaudhry, M. A., Nie, Y., Xie, Z., Shapiro, J. I., Liu, J. (2017). A mouse 5/6th nephrectomy model that induces experimental uremic cardiomyopathy. *J Vis Experim* 129, 1–6. doi: 10.3791/55825.

Webster, A. C., Nagler, E. V., Morton, R. L., Masson, P. (2017). Chronic Kidney Disease. *Lancet* 389, 1238–1252. doi: 10.1016/S0140-6736(16)32064-5.

Wiklander, O. P. B., Bostancioglu, R. B., Welsh, J. A., Zickler, A. M., Murke, F., Corso, G., et al. (2018). Systematic methodological evaluation of a multiplex bead-based flow cytometry assay for detection of extracellular vesicle surface signatures. *Front Immunol* 9. doi: 10.3389/fimmu.2018.01326.

Zucker, S., Wieman, J. M., Lysik, R. M., et al. (1987). Metastatic mouse melanoma cells release collagen-gelatin degrading metalloproteinases as components of shed membrane vesicles. *Biochim Bioph Acta* 924(1), 225–237. doi: 10.1016/0304-4165(87)90091-2.

APPENDIX 1

During my PhD, the research activity has been mainly focused on research projects that aimed to study the anti-fibrotic and anti-inflammatory effects of Extracellular Vesicles (EVs) isolated from stem cells. In our group, we have been mainly concentrated on EVs isolated from Mesenchymal Stem Cells (MSCs) and Human Liver Stem Cells (HLSCs), trying to understand the molecular mechanisms at the base of their anti-fibrotic properties. To achieve this objective, in the last years we have developed different murine model of renal and liver fibrosis, but also *in vitro* models of liver fibrosis.

During my PhD experience, I took part to same of these research activities which have been also published in international journals.

One of the first projects (**Figure 14**) regards the study of the therapeutic potential of EVs derived from HLSCs in a murine model of Ischemia Reperfusion Injury (IRI)-induced Chronic Kidney Disease (CKD).

International Journal of *Molecular Sciences*

MDPI

Article

Extracellular Vesicles Derived from Human Liver Stem Cells Attenuate Chronic Kidney Disease Development in an In Vivo Experimental Model of Renal Ischemia and Reperfusion Injury

Stefania Bruno [1,2,*,†], Giulia Chiabotto [1,†], Massimo Cedrino [2,3], Elena Ceccotti [1], Chiara Pasquino [1,2], Samuela De Rosa [1], Cristina Grange [1,2], Stefania Tritta [2] and Giovanni Camussi [1,2]

[1] Department of Medical Sciences, University of Torino, 10126 Torino, Italy; giulia.chiabotto@unito.it (G.C.); elena.ceccotti@unito.it (E.C.); chiara.pasquino@unito.it (C.P.); samuela.derosa@edu.unito.it (S.D.R.); cristina.grange@unito.it (C.G.); giovanni.camussi@unito.it (G.C.)
[2] Molecular Biotechnology Center, University of Torino, 10126 Torino, Italy; massimo.cedrino@unito.it (M.C.);

Abstract: The potential therapeutic effect of extracellular vesicles (EVs) that are derived from human liver stem cells (HLSCs) has been tested in an in vivo model of renal ischemia and reperfusion injury (IRI), that induce the development of chronic kidney disease (CKD). EVs were administered intravenously immediately after the IRI and three days later, then their effect was tested at different time points to evaluate how EV-treatment might interfere with fibrosis development. In IRI-mice that were sacrificed two months after the injury, EV- treatment decreased the development of interstitial fibrosis at the histological and molecular levels. Furthermore, the expression levels of pro-inflammatory genes and of epithelial–mesenchymal transition (EMT) genes were significantly reverted by EV-treatment. In IRI-mice that were sacrificed at early time points (two and three days after the injury), functional and histological analyses showed that EV-treatment induced an amelioration of the acute kidney injury (AKI) that was induced by IRI. Interestingly, at the molecular level, a reduction of pro-fibrotic and EMT-genes in sacrificed IRI-mice was observed at days two and three after the injury. These data indicate that in renal IRI, treatment with HLSC-derived EVs improves AKI and interferes with the development of subsequent CKD by modulating the genes that are involved in fibrosis and EMT.

Figure 14. Abstract of the paper *Bruno S. et a. Extracellular Vesicles Derived from Human Liver Stem Cells Attenuate Chronic Kidney Disease Development in an In Vivo Experimental Model of Renal Ischemia and Reperfusion Injury. Int. J. Mol. Sci. 2022.* DOI: https:// doi.org/10.3390/ijms23031485.

The injection of two doses of HLSC-EVs soon after the injury ameliorate Acute Kidney Injury (AKI) and interferes with CKD progression both at functional and histological levels. Interestingly, at the molecular level, HLSC-EVs modulate the expression of pro-fibrotic, pro-inflammatory and epithelial-mesenchymal transition (EMT) genes, which are involved in disease progression.

In the context of liver fibrosis, our group have previously demonstrated how HLSC-EVs attenuate liver fibrosis and inflammation in a mouse model of non-alcoholic steatohepatitis (NASH) *(Bruno S. et al. 2020).* More recently, we have developed an *in vitro* model of liver fibrosis using a human hepatic stellate cell line (LX-2) activated by a strong pro-fibrotic stimulus such as transforming growth factor-beta 1 (TGF-b1) (**Figure 15**). From the literature we know that activated hepatic stellate cells (HSCs) act as key drivers of liver fibrosis and we investigated the effects of HLSC-derived EVs on activated LX-2. The results of this work allowed us to deeply investigate the mechanism of action of HLSC-EVs which can target LX-2 and attenuate their activated phenotype by down-regulating the expression of the pro-fibrotic marker Alpha-Smooth Muscle Actin (α-SMA).

Interestingly, HLSC-EV biological effect can be mediated by the releasing in activated HSCs of anti-fibrotic miRNAs, such as miR-146a-5p.

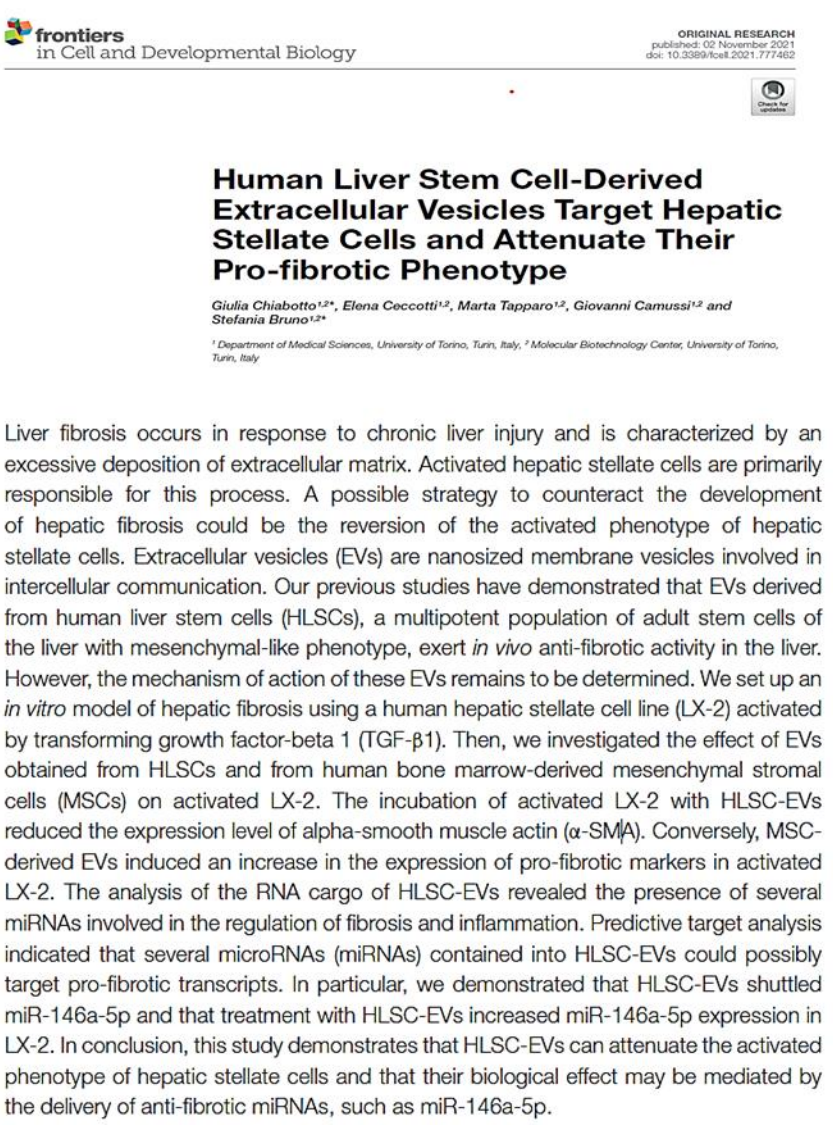

frontiers in Cell and Developmental Biology

ORIGINAL RESEARCH
published: 02 November 2021
doi: 10.3389/fcell.2021.777462

Human Liver Stem Cell-Derived Extracellular Vesicles Target Hepatic Stellate Cells and Attenuate Their Pro-fibrotic Phenotype

Giulia Chiabotto[1,2], Elena Ceccotti[1,2], Marta Tapparo[1,2], Giovanni Camussi[1,2] and Stefania Bruno[1,2]**

[1] Department of Medical Sciences, University of Torino, Turin, Italy, [2] Molecular Biotechnology Center, University of Torino, Turin, Italy

Liver fibrosis occurs in response to chronic liver injury and is characterized by an excessive deposition of extracellular matrix. Activated hepatic stellate cells are primarily responsible for this process. A possible strategy to counteract the development of hepatic fibrosis could be the reversion of the activated phenotype of hepatic stellate cells. Extracellular vesicles (EVs) are nanosized membrane vesicles involved in intercellular communication. Our previous studies have demonstrated that EVs derived from human liver stem cells (HLSCs), a multipotent population of adult stem cells of the liver with mesenchymal-like phenotype, exert *in vivo* anti-fibrotic activity in the liver. However, the mechanism of action of these EVs remains to be determined. We set up an *in vitro* model of hepatic fibrosis using a human hepatic stellate cell line (LX-2) activated by transforming growth factor-beta 1 (TGF-β1). Then, we investigated the effect of EVs obtained from HLSCs and from human bone marrow-derived mesenchymal stromal cells (MSCs) on activated LX-2. The incubation of activated LX-2 with HLSC-EVs reduced the expression level of alpha-smooth muscle actin (α-SMA). Conversely, MSC-derived EVs induced an increase in the expression of pro-fibrotic markers in activated LX-2. The analysis of the RNA cargo of HLSC-EVs revealed the presence of several miRNAs involved in the regulation of fibrosis and inflammation. Predictive target analysis indicated that several microRNAs (miRNAs) contained into HLSC-EVs could possibly target pro-fibrotic transcripts. In particular, we demonstrated that HLSC-EVs shuttled miR-146a-5p and that treatment with HLSC-EVs increased miR-146a-5p expression in LX-2. In conclusion, this study demonstrates that HLSC-EVs can attenuate the activated phenotype of hepatic stellate cells and that their biological effect may be mediated by the delivery of anti-fibrotic miRNAs, such as miR-146a-5p.

Figure 15. Abstract of the paper *Chiabotto G. et al. Human liver stem cell-derived extracellular vesicles target hepatic stellate cells and attenuate their pro-fibrotic phenotype.* 2021. DOI: 10.3389/fcell.2021.777462.

To better understand the possible mechanism of action of HLSC-EVs in the context of liver fibrosis, we concentrated the attention not only on the modulation of pro-fibrotic transcripts but also on other RNA species such as long non-coding RNAs (lncRNAs). Recently it has been highlighted the involvement of lncRNAs in fibrogenesis in different organs; in this work (**Figure 16**) we evaluated whether the therapeutic activity of HLSC-EVs also involves the modulation of inflammation-related lncRNAs in NASH liver and in our *in vitro* model of liver fibrosis (**Figure 15**).

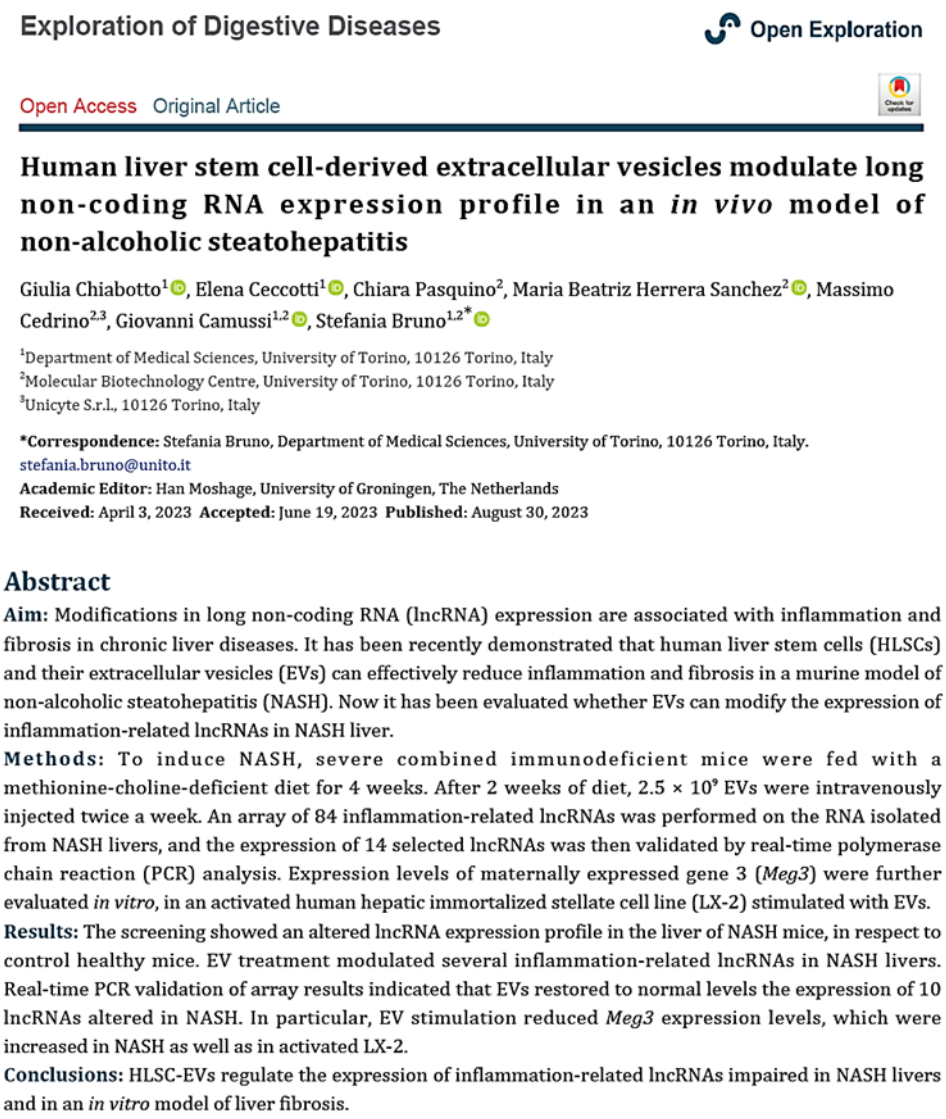

Exploration of Digestive Diseases

Open Exploration

Open Access Original Article

Human liver stem cell-derived extracellular vesicles modulate long non-coding RNA expression profile in an *in vivo* model of non-alcoholic steatohepatitis

Giulia Chiabotto[1], Elena Ceccotti[1], Chiara Pasquino[2], Maria Beatriz Herrera Sanchez[2], Massimo Cedrino[2,3], Giovanni Camussi[1,2], Stefania Bruno[1,2*]

[1]Department of Medical Sciences, University of Torino, 10126 Torino, Italy
[2]Molecular Biotechnology Centre, University of Torino, 10126 Torino, Italy
[3]Unicyte S.r.l., 10126 Torino, Italy

***Correspondence:** Stefania Bruno, Department of Medical Sciences, University of Torino, 10126 Torino, Italy.
stefania.bruno@unito.it
Academic Editor: Han Moshage, University of Groningen, The Netherlands
Received: April 3, 2023 **Accepted:** June 19, 2023 **Published:** August 30, 2023

Abstract

Aim: Modifications in long non-coding RNA (lncRNA) expression are associated with inflammation and fibrosis in chronic liver diseases. It has been recently demonstrated that human liver stem cells (HLSCs) and their extracellular vesicles (EVs) can effectively reduce inflammation and fibrosis in a murine model of non-alcoholic steatohepatitis (NASH). Now it has been evaluated whether EVs can modify the expression of inflammation-related lncRNAs in NASH liver.

Methods: To induce NASH, severe combined immunodeficient mice were fed with a methionine-choline-deficient diet for 4 weeks. After 2 weeks of diet, 2.5×10^9 EVs were intravenously injected twice a week. An array of 84 inflammation-related lncRNAs was performed on the RNA isolated from NASH livers, and the expression of 14 selected lncRNAs was then validated by real-time polymerase chain reaction (PCR) analysis. Expression levels of maternally expressed gene 3 (*Meg3*) were further evaluated *in vitro*, in an activated human hepatic immortalized stellate cell line (LX-2) stimulated with EVs.

Results: The screening showed an altered lncRNA expression profile in the liver of NASH mice, in respect to control healthy mice. EV treatment modulated several inflammation-related lncRNAs in NASH livers. Real-time PCR validation of array results indicated that EVs restored to normal levels the expression of 10 lncRNAs altered in NASH. In particular, EV stimulation reduced *Meg3* expression levels, which were increased in NASH as well as in activated LX-2.

Conclusions: HLSC-EVs regulate the expression of inflammation-related lncRNAs impaired in NASH livers and in an *in vitro* model of liver fibrosis.

Figure 16. Abstract of the *paper Chiabotto G. et al. Human liver stem cell-derived extracellular vesicles modulate long non-coding RNA expression profile in an in vivo model of non-alcoholic steatohepatitis. Expl. Dig. Dis. 2023.* DOI: https://doi.org/10.37349/edd.2023.00025.

Interestingly, we demonstrated that HLSC-EVs can restore to baseline levels some inflammation-related lncRNAs dysregulated in NASH and activated LX-2, indicating their possible involvement in the therapeutic potential of this EV population in the liver fibrosis.

We have also produced two reviews, one of which gives an overview of the more recent and innovative 2D and 3D models to investigate the mechanism involved in liver fibrosis as an alternative to animal models and to study new possible anti-fibrotic compounds (**Figure 17**). The other one speculated the application of natural or engineered EVs isolated from stem cells to treat different kidney pathologies (**Figure 18**).

Review Article

Narrative review of *in vitro* experimental models of hepatic fibrogenesis

Giulia Chiabotto[1], Elena Ceccotti[1], Stefania Bruno[1,2]

[1]Department of Medical Sciences, University of Torino, Torino, Italy; [2]Molecular Biotechnology Center, University of Torino, Torino, Italy

Contributions: (I) Conception and design: G Chiabotto, S Bruno; (II) Administrative support: None; (III) Provision of study materials or patients: None; (IV) Collection and assembly of data: G Chiabotto, E Ceccotti; (V) Data analysis and interpretation: None; (VI) Manuscript writing: All authors; (VII) Final approval of manuscript: All authors.

Correspondence to: Stefania Bruno, PhD. Department of Medical Sciences, University of Torino, 10126 Torino, Italy. Email: stefania.bruno@unito.it.

Background and Objective: Hepatic fibrosis is a pathological condition affecting millions of people worldwide that results from an improper tissue repair process, following liver injury or inflammation. Since progressive liver fibrosis can evolve into end-stage liver diseases, it is becoming increasingly important to develop efficient experimental models for evaluating new anti-fibrotic therapies. An important role in the onset and progression of hepatic fibrosis is played by hepatic stellate cells (HSCs), perisinusoidal vitamin A-storing cells that, in the presence of pro-fibrogenic stimuli, acquire a myofibroblast-like phenotype with an increased ability to produce extracellular matrix (ECM) components. In this review, we provide an overview of the traditional two-dimensional (2D) systems and of the innovative bioengineered three-dimensional (3D) models that allow for the screening of novel anti-fibrotic therapies.

Methods: Data presented in this narrative review were retrieved from scientific literature by searching the computerized database PubMed and MEDLINE for original and review papers describing different *in vitro* 2D and 3D culture systems that mimic hepatic fibrosis.

Key Content and Findings: Over the past years, most *in vitro* studies have focused on the mechanisms underlying HSC activation, using liver cells cultured in traditional 2D systems. The development of 3D *in vitro* models allowed studying the complex interactions between HSCs and the surrounding parenchymal and non-parenchymal cells, and between liver cells and ECM, thus improving the mimicking of the situation *in vivo*. Advanced bioengineered 3D models can replace *in vivo* models reducing the ethical concerns and biological issues.

Conclusions: Traditional and innovative *in vitro* cell culture systems represent a valid alternative to *in vivo* animal models in the investigation of the complex mechanisms involved in fibrosis development and in the discovery of new anti-fibrogenic compounds for the treatment of hepatic fibrosis.

Figure 17. Abstract of the paper *Chiabotto G. et al. Narrative review of in vitro experimental models of hepatic fibrogenesis. Dig. Med. Res. 2022.* DOI: https://dx.doi.org/10.21037/dmr-21-102.

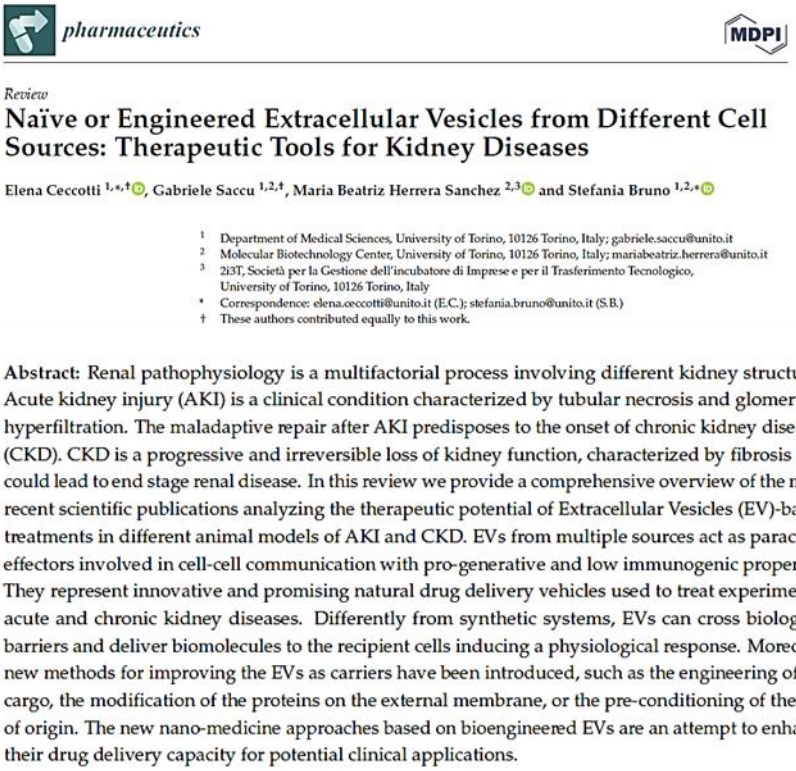

pharmaceutics

MDPI

Review

Naïve or Engineered Extracellular Vesicles from Different Cell Sources: Therapeutic Tools for Kidney Diseases

Elena Ceccotti [1,*,†], Gabriele Saccu [1,2,†], Maria Beatriz Herrera Sanchez [2,3] and Stefania Bruno [1,2,*]

[1] Department of Medical Sciences, University of Torino, 10126 Torino, Italy; gabriele.saccu@unito.it
[2] Molecular Biotechnology Center, University of Torino, 10126 Torino, Italy; mariabeatriz.herrera@unito.it
[3] 2i3T, Società per la Gestione dell'incubatore di Imprese e per il Trasferimento Tecnologico, University of Torino, 10126 Torino, Italy
* Correspondence: elena.ceccotti@unito.it (E.C.); stefania.bruno@unito.it (S.B.)
† These authors contributed equally to this work.

Abstract: Renal pathophysiology is a multifactorial process involving different kidney structures. Acute kidney injury (AKI) is a clinical condition characterized by tubular necrosis and glomerular hyperfiltration. The maladaptive repair after AKI predisposes to the onset of chronic kidney diseases (CKD). CKD is a progressive and irreversible loss of kidney function, characterized by fibrosis that could lead to end stage renal disease. In this review we provide a comprehensive overview of the most recent scientific publications analyzing the therapeutic potential of Extracellular Vesicles (EV)-based treatments in different animal models of AKI and CKD. EVs from multiple sources act as paracrine effectors involved in cell-cell communication with pro-generative and low immunogenic properties. They represent innovative and promising natural drug delivery vehicles used to treat experimental acute and chronic kidney diseases. Differently from synthetic systems, EVs can cross biological barriers and deliver biomolecules to the recipient cells inducing a physiological response. Moreover, new methods for improving the EVs as carriers have been introduced, such as the engineering of the cargo, the modification of the proteins on the external membrane, or the pre-conditioning of the cell of origin. The new nano-medicine approaches based on bioengineered EVs are an attempt to enhance their drug delivery capacity for potential clinical applications.

Figure 18. Abstract of the paper *Ceccotti E. et al. Naïve or Engineered Extracellular Vesicles from Different Cell Sources: Therapeutic Tools for Kidney Diseases. Pharm. 2023*. DOI: https://doi.org/10.3390/ pharmaceutics15061715.

APPENDIX 2

During my PhD, I had the opportunity to take part in different national and international conferences. The followings are the oral communications I have presented:

1. ISEV Annual Meeting (Lyon, May 2022). Abstract title: "Human liver stem cell-derived extracellular vesicles interfere with the development of chronic kidney disease in an in vivo experimental model of renal ischemia and reperfusion injury".

2. EVIta Workshop "EV Connect: fostering collaboration" (Torino, September 2022). Abstract title: "Extracellular vesicles derived from human liver stem cells modulated the expression of epithelial-mesenchymal transition genes in an *in vivo* experimental model of renal ischemia and reperfusion injury".

3. GISM (Torino, October 2022). Abstract title: "Human liver stem cell-derived extracellular vesicles interfere with the development of chronic kidney disease in an *in vivo* experimental model of renal ischemia and reperfusion injury".

4. EVIta Symposium (Urbino, September 2023). Abstract title: "Extracellular vesicles derived from human liver stem cells counteract Chronic Kidney Disease development and Cardiac Dysfunction in remnant kidney murine model".

Acknowledgments

Arrivata alla fine di questo percorso, ho il piacere e il dovere di scrivere questi ringraziamenti. Ho la fortuna di ringraziare tante persone fantastiche che mi sono state vicine.

Il primo grande 'grazie' lo dedico a Giulia e Stefania che mi hanno accolto nel loro laboratorio quando la pandemia ha cambiato alcune carte in tavola. Da voi ho potuto imparare tanto e mi avete altrettanto supportata, creando un piccolo grande team di ricerca.

Massimo, un altro ringraziamento speciale va a te. Senza di te e la tua abilità nel fare le chirurgie tutto questo lavoro non sarebbe stato fattibile.

Voglio ringraziare i miei genitori perché mi hanno sempre supportata e hanno da sempre fatto sacrifici per rendere realizzabile tutto quanto, spero di rendervi orgogliosi raggiungendo questo traguardo.

Alla mia famiglia, ai miei super nonni, ai fantastici zii e cugini; ad uno ad uno vi ringrazio immensamente per esserci sempre stati e per avermi fatto sentire il vostro affetto.

Grazie al gruppo dell'MBC, alle persone che durante questo percorso mi hanno aiutata e che hanno contribuito a questo progetto. In particolare, Sarah, Adele e Roberta, 'le cugine di lab', siete state compagne di convegni, di confronti su esperimenti non riusciti o anche solo di sfoghi liberatori.

Sara, Malvina e Alessandro, 'i ragazzi Brizzi', in questi anni siete stati un vero punto di riferimento e di supporto dentro e fuori il laboratorio.

Federica e Lucia, con voi si è creato un rapporto davvero speciale che ormai continua anche al di fuori delle Molinette. Siete state sempre presenti e pronte a consolarmi con qualche foto di gatti.

Non può mancare un ringraziamento per le mie amiche marchigiane, Ilaria, Giulia, Giorgia, Martina, Amy e Valeria, ci conosciamo ormai da una vita e nonostante la distanza ci siete sempre state e ogni volta non vedo l'ora di scrivervi 'prossimo weekend sono giù, cosa facciamo?'.

Francesco M., Francesco G. e Simone, voi siete una forza della natura e tra gite a Torino, messaggi e chiamate siete sempre stati presenti. Un ringraziamento ve lo meritate tutto!

Le fantastiche ragazze del Gruppo Terrone Torinesi, Linda e Federica, voi siete state il mio porto sicuro sin dal primo giorno a Torino. Grazie per essermi state a fianco e per aver sempre ricordato quella ‘casa’ che a volte manca un po'.

Poi vorrei ringraziare le fantastiche persone che ho conosciuto a Torino e delle quali ormai non posso fare a meno. Marti, Tina, Miriam e la nostra londinese Bea, oltre che condividere la passione per i gatti e per la scienza, abbiamo condiviso così tanto durante questo percorso. Siete delle persone speciali, grazie per tutto!

Infine, vorrei ringraziare Antonio, Lucrezia e Luca. Mi avete sempre fatto sentire parte della famiglia; mi avete accolta durante il COVID e soprattutto mi avete sfamata!

Il gruppo 'amici di Mattia' che presto sono diventati amici a tutti gli effetti anche per me. Fede, Ale, Sicu, Vittoria, Sam e Riccardo, vorrei dedicare un 'grazie' anche a voi. Ci consociamo ormai da qualche anno e anche voi avete reso questi anni ricchi di tante esperienze bellissime.

C’è poi la ‘persona’ che forse più di tutti mi ha sopportata in questo percorso e che mi ha sempre spronata ripetendo, cito testuali parole, 'sei tu quella che farà i big money!’. A parte gli scherzi, grazie per tutto e per non essere scappato via!

Grazie a tutti quelli che hanno avuto la pazienza di leggere fino alla fine, scusate ma dovevo farlo. Grazie a chi mi ha supportata con il pensiero e chi lo ha fatto da lassù.

Grazie anche un po' a me stessa per non aver mollato.